International Journal of Applied Earth Observations and Geoinformation 96 (2021) 102277

Contents lists available at ScienceDirect

International Journal of Applied Earth Observations and Geoinformation

journal homepage: www.elsevier.com/locate/jag

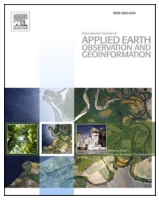

Temporal mosaicking approaches of Sentinel-2 images for extending topsoil organic carbon content mapping in croplands

Emmanuelle Vaudour [a,*], Cécile Gomez [b,c], Philippe Lagacherie [b], Thomas Loiseau [d], Nicolas Baghdadi [e], Diego Urbina-Salazar [a], Benjamin Loubet [a], Dominique Arrouays [d]

[a] Université Paris-Saclay, INRAE, AgroParisTech, UMR ECOSYS, 78850 Thiverval-Grignon, France
[b] LISAH, Univ. Montpellier, INRAE, IRD, Montpellier Supagro, Montpellier, France
[c] Indo-French Cell for Water Sciences, IRD, Indian Institute of Science, Bangalore 560012, India
[d] INRAE, InfoSol Unit, US 1106, 45075 Orléans, France
[e] INRAE, University of Montpellier, UMR TETIS, 500 rue François Breton, 34093 Montpellier CEDEX 5, France

ARTICLE INFO

Keywords:
Soil organic carbon
Sentinel-2
Temporal mosaic
Croplands
Soil moisture

ABSTRACT

The spatial assessment of soil organic carbon (SOC) is a major environmental challenge, notably for evaluating soil carbon stocks. Recent works have shown the capability of Sentinel-2 to predict SOC content over temperate agroecosystems characterized with annual crops. However, because spectral models are only applicable on bare soils, the mapping of SOC is often obtained on limited areas. A possible improvement for increasing the number of pixels on which SOC can be retrieved by inverting bare soil reflectance spectra, consists of using optical images acquired at several dates. This study compares different approaches of Sentinel–2 images temporal mosaicking to produce a composite multi-date bare soil image for predicting SOC content over agricultural topsoils. A first approach for temporal mosaicking was based on a per-pixel selection and was driven by soil surface characteristics: bare soil or dry bare soil with/without removing dry vegetation. A second approach for creating composite images was based on a per-date selection and driven either by the models performance from single-date, or by average soil surface indicators of bare soil or dry bare soil. To characterize soil surface, Sentinel-1 (S1)-derived soil moisture and/or spectral indices such as normalized difference vegetation index (NDVI), Normalized Burn Ratio 2 (NBR2), bare soil index (BSI) and a soil surface moisture index (S2WI) were used either separately or in combination. This study highlighted the following results: i) none of the temporal mosaic images improved model performance for SOC prediction compared to the best single-date image; ii) of the per-pixel approaches, temporal mosaics driven by the S1-derived moisture content, and to a lesser extent, by NBR2 index, outperformed the mosaic driven by the BSI index but they did not increase the bare soil area predicted; iii) of the per-date approaches, the best trade-off between predicted area and model performance was achieved from the temporal mosaic driven by the S1-derived moisture content ($R^2 \sim 0.5$, RPD ~ 1.4, RMSE ~ 3.7 g.kg^{-1}) which enabled to more than double (*2.44) the predicted area. This study suggests that a number of bare soil mosaics based on several indicators (moisture, bare soil, roughness…), preferably in combination, might maintain acceptable accuracies for SOC prediction whilst extending over larger areas than single-date images.

1. Introduction

There is a growing need to update and monitor soil organic carbon (SOC) content over territories, recently emphasized through the 4p1000 initiative (Arrouays and Horn, 2019; Minasny et al., 2017). This holds especially true for topsoil, which is directly impacted by tillage practices and receives organic amendments.

Because the standard method for soil C content measurement is both time-consuming and expensive, alternative approaches have emerged, relying on proximal sensing, and by extension, on remote sensing. As a matter of fact, soil reflectance is strongly influenced by SOC: empirical spectral models relating SOC content to reflectance have been successfully built, from lab spectra (eg. Viscarra-Rossel et al., 2006), but also over bare soils from airborne hyperspectral image spectra of bare soils (Selige et al., 2006; Stevens et al., 2010; Vaudour et al., 2016), and more recently, from bare soils image spectra acquired by the new generation

* Corresponding author.
E-mail address: Emmanuelle.Vaudour@agroparistech.fr (E. Vaudour).

https://doi.org/10.1016/j.jag.2020.102277
Received 29 June 2020; Received in revised form 13 November 2020; Accepted 30 November 2020
Available online 14 December 2020

multispectral Sentinel-2 satellites (Gholizadeh et al., 2018; Castaldi et al., 2019a, b; Vaudour et al., 2019a,b; Žížala et al., 2019).

Launched in 2015 and then 2017 Sentinel-2 satellites (S2A and S2B, respectively) provide time series with frequent revisit every 5 days, while their MultiSpectral Instrument (MSI) has more spectral bands (13) than previous multispectral satellite sensors, covering the visible near-infrared shortwave infrared range (400–2500 nm). S2 data are imaged over large areas with a 290 km-swath width, at a spatial resolution of either 10 m (490, 560, 665, 842 nm-central wavelengths) or 20 m (705, 740, 783, 842, 865, 1610, 2190 nm-central wavelengths).

Although Sentinel-2 images are relevant for predicting SOC content for annual crop soils, at least at certain adequately targeted dates (Vaudour et al., 2019b), the area that is likely to be predicted at a given single date is limited as many pixels are covered with crop vegetation. This is the reason why there is a need to investigate the possibility for increasing the predicted area by stacking several dates into a composite image. Recent attempts used Landsat time series at national scales of Switzerland (Diek et al., 2017) or Germany (Rogge et al., 2018) or over large regions of Southeastern Brazil (Demattê et al., 2018; Gallo et al., 2018). Particularly, at the scale of the national territory of Switzerland, Diek et al. (2017) used Landsat time series over several years to make soil composites with largest bare areas, and concluded that such mosaics were very encouraging for further studies about soil property prediction at a larger, continental scale. In a similar attempt, Loiseau et al. (2019) elaborated a mosaic of Sentinel-2 at the scale of mainland France, and incorporated the reflectance and spectral indices computed from it into a larger set of non-spectral covariates and other spectral covariates (such as derived from MODIS) to predict topsoil clay content. They found that incorporating Sentinel-2 data contributed to slightly improve the predicting performance for clay content.

These previous studies relied on varied approaches for elaborating the multidate mosaic image of bare soil area, in turn named “barest soil composite” (Diek et al. 2017), “mosaic of exposed soils” (Rogge et al., 2018), “synthetic soil image” (Demattê et al., 2018), “bare soil composite image” (Gallo et al., 2018), or “bare soil mosaic” (Loiseau et al., 2019). Besides atmospheric correction and the masking of clouds and cloud shadows, that all these previous studies share (with variants), the common procedure of these approaches relied on the empirical definition of a spectral index threshold in order to discriminate between bare soil and vegetated surface, and in some cases urban surfaces. Nevertheless, they covered large spatial extent and had no specific focus on agricultural soils, by means of land parcel register. The spectral index used for sieving the bare soils pixels were either the normalized difference vegetation index (NDVI) (Rogge et al., 2018; Loiseau et al., 2019) or the so-called “bare soil index” (BSI) (Diek et al., 2017) or the NDVI jointly to the mid infrared index “Normalized Burn Ratio 2” (NBR2) (Demattê et al., 2018, 2020; Gallo et al., 2018; Castaldi et al., 2019b; Tziolas et al., 2020) (see §2.6 for index formulae).

When carrying out a multidate mosaic, the pixels of such a mosaic have a reflectance spectrum of bare soil, each originating from different dates acquired in contrasted soil surface conditions of soil moisture, roughness, green or dry vegetation cover that vary over time. Approaches including the NBR2 index into the process chain for bare soil compositing have relied on Landsat8 series (Demattê et al., 2018, 2020; Gallo et al., 2018) and the NBR2 index was used to account for the presence of dry vegetation on surface. As a matter of fact, the NBR2 index was initially defined by Van Deventer et al. (1997) as “Normalized Difference Tillage index” (NDTI) for the Landsat TM, to detect crop residue cover for conservation tillage fields. As recently demonstrated from Sentinel-2, crop residue cover as characterized through the NBR2 index leads to deteriorating SOC prediction performance (Castaldi et al., 2019b). However, soil moisture might also worsen SOC prediction models, as verified in lab conditions (Minasny et al., 2011; Rienzi et al., 2014); yet, none of these previous approaches has accounted for the specific influence of soil moisture. Relying on a previously studied Sentinel-2 time series, for which the SOC prediction performances have been compared for single dates (Vaudour et al., 2019b), the present study intends to account for soil moisture information for the purpose of multidate mosaicking and raises two main questions: i) to what degree a multidate composite image performs well for cultivated soils with annual crops and rotating bare soil area; ii) in such specific agro-ecosystem, what is the optimal elaboration strategy for scoring best performance of SOC content prediction and should it rely on incorporating soil moisture information? (Rienzi et al., 2014).

The term “mosaicking” might refer to the spatial juxtaposition of several image tiles, or else to the spatio-temporal combination of several multidate images within a same tile, or both.

The present paper deals with two main approaches for the spatio-temporal combination of several multidate images into a composite image within a same tile, hereby referred to as “temporal mosaicking”: either “per-pixel”, i.e. computed on the base of each pixel vector of values across the time series, or “per date”, i.e. relying on a global indicator per date. Both sets of mosaics were driven by soil surface characteristics: bare soil, or dry soil, or both. To characterize soil surface, Sentinel-1 (S1)-derived soil moisture and/or spectral indices such as normalized difference vegetation index (NDVI), Normalized Burn Ratio 2 (NBR2), bare soil index (BSI) and a soil surface moisture index (S2WI) were used either separately or in combination. Per-pixel mosaics were driven by either “bare soil”, obtained from least NDVI, least NBR2 or highest BSI value; or “driest soil”, derived from least soil moisture S2WI index or least S1-derived estimated water content applied to bare soil. Per date mosaics were driven by either the best single prediction performance by decreasing order amongst dates (“best date”), or the least average NBR2 index value amongst several dates (“bare date”), or the least average soil moisture index or value amongst several available dates (“driest date”).

2. Materials and methods

2.1. Study area: The Versailles Plain

The Versailles Plain, or ‘*Plaine de Versailles*’, located west of Paris (North of France, 48°46′-48°56′N; 1°50′-2°07′E) is in the NW-SE view of the esplanade of the Palace of Versailles and covers a total extent of 221 km2, of which about half (105.65 km2 in 2017) undergoes intensive annual crop cultivation (Vaudour et al., 2016) (Fig. 1). The main crop rotations in the area involve winter wheat, winter rapeseed, winter and spring barley and maize on occasion. As cultivation practices are mainly conventional, with early winter ploughing applied at least 1 year out of every 3, it can be assumed that topsoil SOC is homogenized by ploughing. Crop rotations last three or four years in average. Landforms are either flat or gently sloping, and structured into a lower limestone plateau at ~120-m elevation in the center and an upper millstone clay plateau at ~170-m elevation along the northern and southern edges of the area. Quaternary loessic deposits and loessic colluvium leave a mark everywhere, and particularly on plateaus, where haplic or glossic luvisols develop according to the FAO classification (World Reference Base WRB, 2014; Crahet, 1992; Vaudour et al., 2019a,b) (Fig. 2).

Arenic cambisols develop from the Fontainebleau acid sands across the largely forested upper plateau flanks, while calcaric cambisols derive from limestone, and colluvial surficial formations are observed in the lower plateau flanks. Along the lower slopes and at the valley bottoms, stagnic colluvic cambisols originate from marls, alluvio-colluvial materials or chalk. Highest SOC values are located in the valley bottoms, followed by lower slopes, then lower plateau, while the lowest contents characterize the higher plateau, followed by those of the plateau flanks (Zaouche et al., 2017) (Fig. 2).

2.2. Sentinel-2 time series

A Sentinel-2A time-series was gathered, initially composed of 13 dates corresponding to a maximum coverage of bare soil, from 1 March

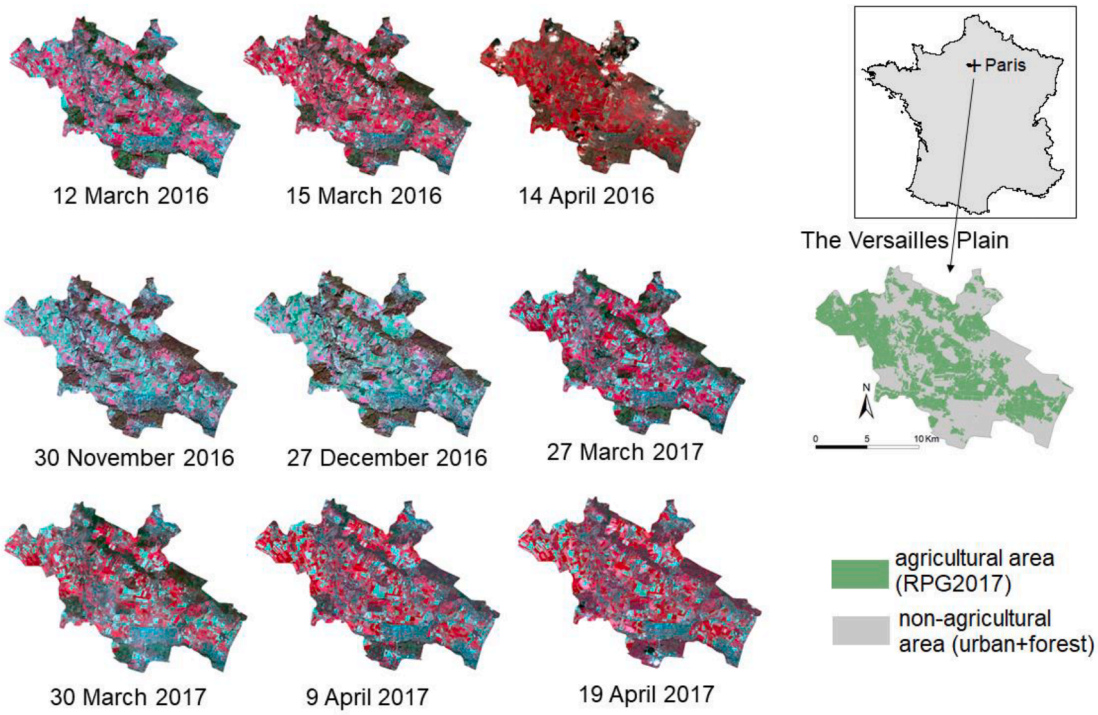

Fig. 1. Agricultural area of the Versailles Plain and infrared coloured images (RGB = B8, B4, B3) of the Sentinel-2 time series gathered for this study. RPG2017 (for *Registre Parcellaire Graphique 2017*) is the Land Parcel Registry map composed of the 2017 crops declared by farmers in the framework of the European Common Agricultural Policy.

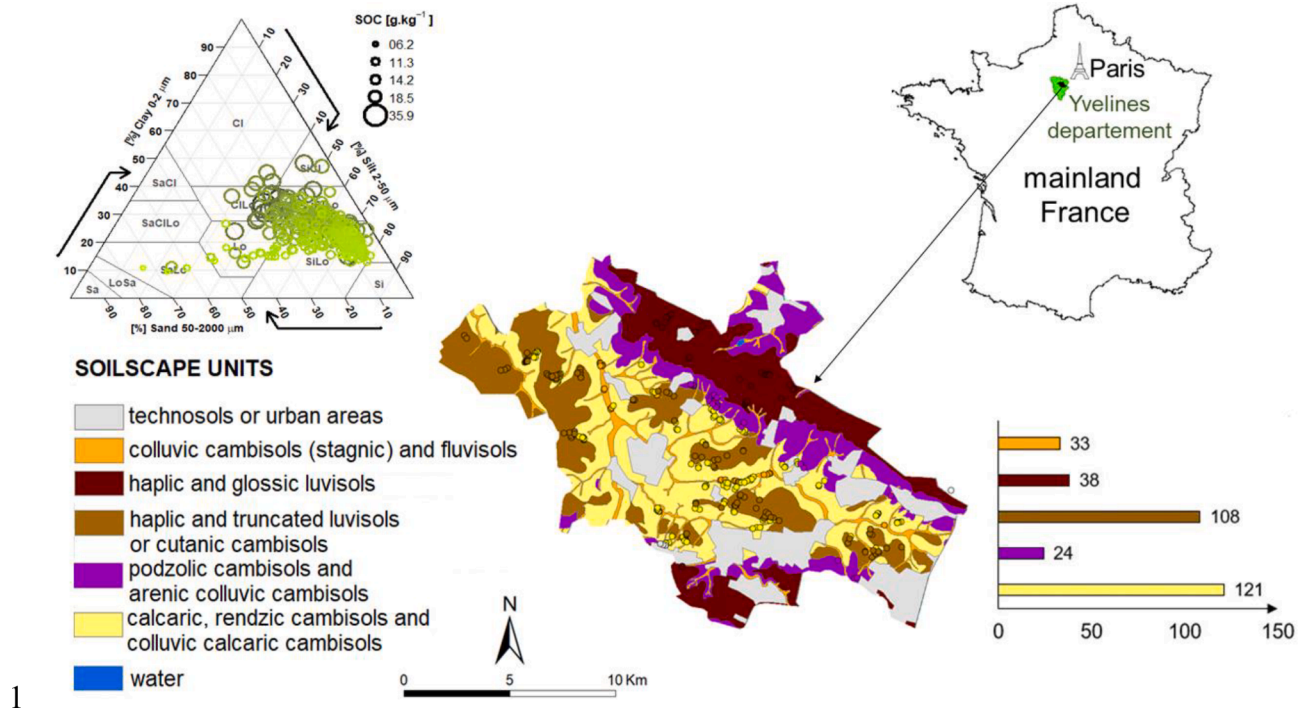

Fig. 2. Soilscape map of the study area, main soil types and distribution of soil samples according to the soilscape units and the soil texture triangle (larger circles indicate higher SOC contents).

to 30 April in 2016 and 2017 and 1 November to 31 December in 2016. For each date, ten atmospherically corrected bands with correction of slope effects were downloaded from the Muscate platform of the French land data center, called Théia (Theia.cnes.fr, 2018) in Level-2A processing at 10 or 20 m resolution (Band: 2, 3, 4, 5, 6, 7, 8, 8A, 11, 12, Table 1), then stacked with 10 m resolution.

A so-called "geophysical mask" (masque *géophysique* or MG2) is provided together with the images and enables to remove clouds, cloud and topographical shadows (Baetens et al., 2019). The images differed in terms of cloud and shadow cover, which ranged from null to almost

Table 1
Specifications of Sentinel-2A MultiSpectral Instrument sensor (in bold characters, bands provided by the Muscate platform).

Spectral band	Spectral domain	Central wavelength (nm)	Bandwidth (nm)	Spatial resolution (m)
B1	Vis	443	20	60
B2	**Vis**	**490**	**65**	**10**
B3	**Vis**	**560**	**35**	**10**
B4	**Vis**	**665**	**30**	**10**
B5	**R-edge**	**705**	**15**	**20**
B6	**R-edge**	**740**	**15**	**20**
B7	**R-edge**	**783**	**20**	**20**
B8	**NIR**	**842**	**115**	**10**
B8A	**NIR**	**865**	**20**	**20**
B9	NIR	945	20	60
B10	SWIR	1380	30	60
B11	**SWIR**	**1610**	**90**	**20**
B12	**SWIR**	**2190**	**180**	**20**

Vis, visible; R-edge, red edge; NIR, near infrared; SWIR, shortwave infrared

85.5% within the entire tile, and from null to nearly 100% at the very location of the study area. Therefore, four images were removed from the time series because of their too large cloud and shadow coverage and we finally retained 9 images (Table 2, Fig. 1).

2.3. Soil moisture series derived from Sentinel-1

Nine soil moisture maps with 10 m-resolution provided by the Theia platform (https://www.theia-land.fr/en/product/soil-moisture-with-very-high-spatial-resolution) were selected as close as possible to the Sentinel-2 acquisition dates (Table 3).

The Sentinel-1/Sentinel-2-derived soil moisture product at plot scale (S2MP) is obtained by coupling Sentinel-1 SAR data and Sentinel-2 optical data. The S2MP product provides soil moisture estimates over the agricultural areas at plot scale with six days revisit time. To estimate the surface soil moisture values (0–10 cm depth), El Hajj et al. (2017) inverted the Water Cloud Model (WCM) parameterized by Baghdadi et al. (2017) for C-band combined with the Integral Equation Model, as modified by Baghdadi et al. (2006). The WCM-inversion approach uses the Neural Network (NN) technique to invert the radar signal into soil moisture value. In addition to Sentinel-1 images characteristics (incidence angle and radar backscattering coefficient), the normalized difference vegetation index (NDVI) derived from Sentinel-2 is used in input to the NN in order to characterize the vegetation cover where it is present. The S2MP maps are produced for agricultural areas (except for vineyards and orchards). Forest and urban areas are masked using the land cover map of Inglada et al. (2017).The S2MP are available in free open access mode via the Theia French Land Data Center (http://www.theia-land.fr/en/thematic-products). Soil moisture is derived with a precision of 6 vol% for agricultural parcels with or without vegetation (El Hajj et al., 2017; Bazzi et al., 2019). In our approach, only the bare S2MP pixels within land parcel register were retained.

The difference $\Delta\theta$ in soil moisture between S1 and S2 imaging dates was assessed for 0–10 cm depth by means of the topsoil volumetric soil moisture monitored daily at the Integrated Carbon Observation System (ICOS, https://www.icos-ri.eu) ecosystem site FR-Gri, located in the middle of the study area (Loubet et al., 2011). This ICOS site pertains the soilscape unit of the lower limestone plateau mainly characterized by haplic or truncated luvisols. Soil moisture was averaged for a 0–10 cm depth by four CS650 (Campbell Scientific, Logan, USA) soil water content reflectometers. The ICOS site was vegetated with wheat at the beginning of stem elongation in March–April 2016, and then with oilseed rape in winter 2016 (~15 cm high) and in spring 2017 (60 to 170 cm high). Though not measured on bare soil, the soil moisture from the ICOS site provided information on the temporal changes in volumetric soil moisture between two close dates.

The number of days separating Sentinel-1 from Sentinel-2 acquisition dates was comprised between zero (3 images acquired the same day) and five at most (Table 3). The difference in soil moisture between a given Sentinel-1/Sentinel-2 pair was assumed to be negligeable, as i) rainfall measured at INRAE Meteorological Station at Thiverval-Grignon (located in the middle of the study area) during this time lapse, was null (most dates) or as little as 10 mm (for 20 March 2016); ii) the $\Delta\theta$ for the FR-Gri ICOS site was comprised between 0 and −4% at 0–10 cm depth.

2.4. Soil samples

This study used 329 topsoil samples collected from 2010 to 2017 for the purposes of earlier studies (e.g. Vaudour et al., 2019a,b). All of the samples were composed of roughly 10 sub-samples collected to a depth of 8 cm from random locations within a 2.7 × 2.7 m square area centered at the sampling plot as recorded at its center using a Trimble Pathfinder®Power DGPS of 50 cm precision (Vaudour et al., 2014a). Such sampling plot size proved suitable for matching soil reflectance spectra measured in the field with 10 m-multispectral satellite radiance while performing empirical atmospheric correction (Vaudour et al., 2014a). Topsoil samples were bulked and air-dried. They were then gently crushed and sieved to 2 mm prior to conventional soil property determinations (Baize and Jabiol, 2011). The SOC content ranged between 6.2 and 35.9 g.kg-1 (mean 15.4 g.kg-1, standard deviation 5.22 g.kg-1, skewness of 0.96). Loam and clay loam textures were dominant, with SOC content all the more higher than the clay content was high (Fig. 2). As most sampled fields i) never receive any organic amendment, or only in very few amounts (Noirot-Cosson et al., 2016) ii) have been cultivated for decades (>30 years) and, as such, might be considered close to steady state having reached the SOC stock equilibrium (Chenu et al., 2018), it can be assumed that SOC content change was negligible over the 7 y-period used for the soil samplings.

2.5. Spectral models of SOC content prediction

The partial least squares regression (PLSR) method was chosen to construct SOC prediction models based on bare soil samples drawn at each mosaic. Details of the PLSR method can be found in Geladi and

Table 2
Main characteristics of the studied scenes (tile TUDQ31).

Imaging date	Time of acquisition (U.T GMT)	Viewing incidence zenith angle (°)	Sun azimuth (°)	Sun elevation (°)	Cloud/shadow cover of the entire tile (%)	Cloud/shadow cover of study area (%)
12 March 2016	10:50:37	<5.1	160.5	36.1	68.6	0.2
15 March 2016	11:01:57	<8.8	153.5	37.8	7.3	0
14 April 2016	10:57:23	≤8.8	163.5	49.5	80.0	46.6
30 November 2016	11:04:18	≤8.8	172.2	18.7	1.7	1.0
27 December 2016	10:55:27	≤5.0	166.9	16.5	4.4	1.0
27 March 2017	10:50:21	≤5.0	160.2	42.0	0.6	0.9
30 March 2017	11:03:34	<8.8	163.5	43.7	29.2	51.9
9 April 2017	11:05:29	≤8.8	163.5	47.3	0	0
19 April 2017	11:06:01	<8.8	163.4	51.2	2.9	0.9

Table 3
Main characteristics of the Sentinel-1 (S1)-derived soil moisture maps. θ: volumetric water content (vol. %), Nbpixθ: number of bare cropland soil pixels (NDVI $\leq$ 0.35) with estimated θ), $\Delta\theta$: measured difference in volumetric water content (vol.%) between S1 and S2 dates at 0–10 cm depth, at the FR-Gri ICOS monitoring site. S1 images used were acquired at 18:00 UT.

Imaging date of the S1 image	Nbpixθ	Mean θ (vol. %)	Min θ (vol. %)	Max θ (vol. %)	Standard deviation of θ (vol.%)	Day difference with S2 (d)	Rainfall (mm) during day difference	$\Delta\theta$ (vol. %)
8 March 2016	70,208	34.1	22.0	37.4	2.7	4	0.0	0
20 March 2016	75,998	21.1	2.2	28.0	5.1	5	10.0	+1
13 April 2016	26,207	18.4	1.6	28.42	5.6	1	3.5	−1
27 November 2016	225,988	26.5	5.0	28.8	2.8	3	0.0	−4
27 December 2016	156,939	26.2	2.0	28.2	3.1	0	0.0	0
27 March 2017	93,140	19.4	1.2	28.2	6.6	0	0.0	0
2 April 2017	51,768	25.1	18.6	35.0	4.1	3	0.0	−3
8 April 2017	53,070	13.5	0.8	27.8	7.0	1	0.5	−1
20 April 2017	42,365	9.8	0.2	26.6	5.3	1	0.5	0

Kowalski (1986) and Wold et al. (2001). For the target SOC content property, a PLSR model was constructed from image reflectance spectra with 10 selected spectral bands (Table 2). The optimal number of latent variables was determined from the prediction residual error sum of squares (PRESS). A leave-one-out cross-validation procedure was applied (Wold, 1978). The quality of model fit was evaluated from the root mean squared error of cross-validation ($RMSE_{CV}$), from the coefficient of determination of cross-validation (R^2cv), from the residual prediction deviation (RPD_{CV}), i.e., the ratio between the standard deviation of the calibration dataset to the $RMSE_{CV}$; and finally, from the ratio of performance to interquartile distance ($RPIQ_{CV}$) (Bellon-Maurel et al., 2010).

For the models enabling the best cross-validation performances for a given number of dates and relying on a sufficient number of samples ($\geq$150), the selected point locations were intersected between models enabling to gather a common dataset. This common dataset was then split into 2/3 calibration and 1/3 validation subsets, according to a random stratified sampling based on measured SOC contents. The root mean squared error of validation ($RMSE_{val}$), the coefficient of determination of validation (R^2_{val}), the validation RPD (RPD_{val}), and RPIQ ($RPIQ_{val}$) were calculated to evaluate the quality of model fit.

PLSR models were used through R version 3.2.1 (R Development Core Team, 2015) employing the "pls" package (Wehrens and Mevik, 2007).

Spectral models were already obtained for single images in a previous study (Vaudour et al., 2019b) (Table 4).

2.6. Methods for temporal mosaicking of bare soil area

To consider cropland soil only, urban and forests were masked using Land Parcel Registry maps (Vaudour et al., 2019a,b). Cropland pixels with normalized difference vegetation index (NDVI) values exceeding an expert-calibrated threshold were masked. The NDVI was retrieved using bands of 842 nm and 665 nm and was used to create a mask of vegetation. Amongst the agricultural area, vegetated or clouded or shadowed pixels were discarded using this mask of vegetation combined with the MG2 mask (Fig. 3).

Two main approaches for multitemporal mosaicking were constructed, either "per-pixel", i.e. computed on the base of each pixel vector of values across the time series, or "per date", i.e. relying on a global indicator per date. Both sets of mosaics were driven by soil surface characteristics: bare soil, or dry soil, or both (Fig. 3, Table 5). To characterize soil surface, Sentinel-1 (S1)-derived soil moisture and/or spectral indices such as normalized difference vegetation index (NDVI), Normalized Burn Ratio 2 (NBR2), bare soil index (BSI) and a soil surface moisture index (S2WI) were used either separately or in combination. Per-pixel mosaics were driven by either "bare soil", obtained from least NDVI, least NBR2 or highest BSI value; or "driest soil", derived from least soil moisture S2WI index or least S1-derived estimated water content applied to bare soil. Per date mosaics were driven by either the best single prediction performance by decreasing order amongst dates ("best date"), or the least average NBR2 index value amongst several dates ("bare date"), or the least average soil moisture index or value amongst several available dates ("driest date").

2.6.1. Per-pixel approaches

The pixelwise or 'per-pixel' approach implies that each temporal mosaic be composed of pixels selected on an individual basis, which thus may represent a high number of dates, with varied soil surface conditions due to their temporal diversity.

2.6.1.1. Bare soil approaches. A first set of mosaics, named "Bare soil" rely on minimizing a vegetation index (NDVI, equation (1)) or a crop residue index (NBR2, equation (2)) or maximizing a bare soil index (BSI, equation (3)), in order to get the pixels most likely to be bare across the time series.

$$NDVI = \frac{\rho_{NIR} - \rho_{Red}}{\rho_{NIR} + \rho_{Red}} \quad (1)$$

Table 4
Sentinel-2 (S2) cross-validation performance of SOC content prediction by date (in bold characters, intermediate performance)—NDVI > 0.35.

Imaging date	Number of samples	Number of latent variables	$RMSE_{CV}$ (g.kg^{-1})	R^2_{CV}	RPD_{CV}	$RPIQ_{CV}$	Area covered (km^2) for NDVI $\leq$ 0.35	Average NBR2 amongst samples	Average S2WI amongst samples
12 March 2016	83	3	4.78	0.16	1.10	1.60	17.07	0.117	−0.445
15 March 2016	84	5	3.79	0.48	**1.39**	2.06	18.55	0.079	−0.403
14 April 2016	54	1	5.86	0.005	1.02	1.32	7.90	0.113	−0.305
30 November 2016	199	3	5.07	0.02	1.01	1.43	52.21	0.157	−0.357
27 December 2016	172	6	4.83	0.25	1.16	1.49	37.36		−0.340
27 March 2017	147	4	4.45	0.33	1.23	1.51	24.28	0.091	−0.409
30 March 2017	67	5	5.44	0.35	1.25	1.26	12.76	0.159	
9 April 2017	125	5	3.38	0.46	**1.37**	1.92	19.30	0.049	−0.396-
19 April 2017	122	6	3.02	0.58	**1.54**	2.15	16.24	0.046	−0.441

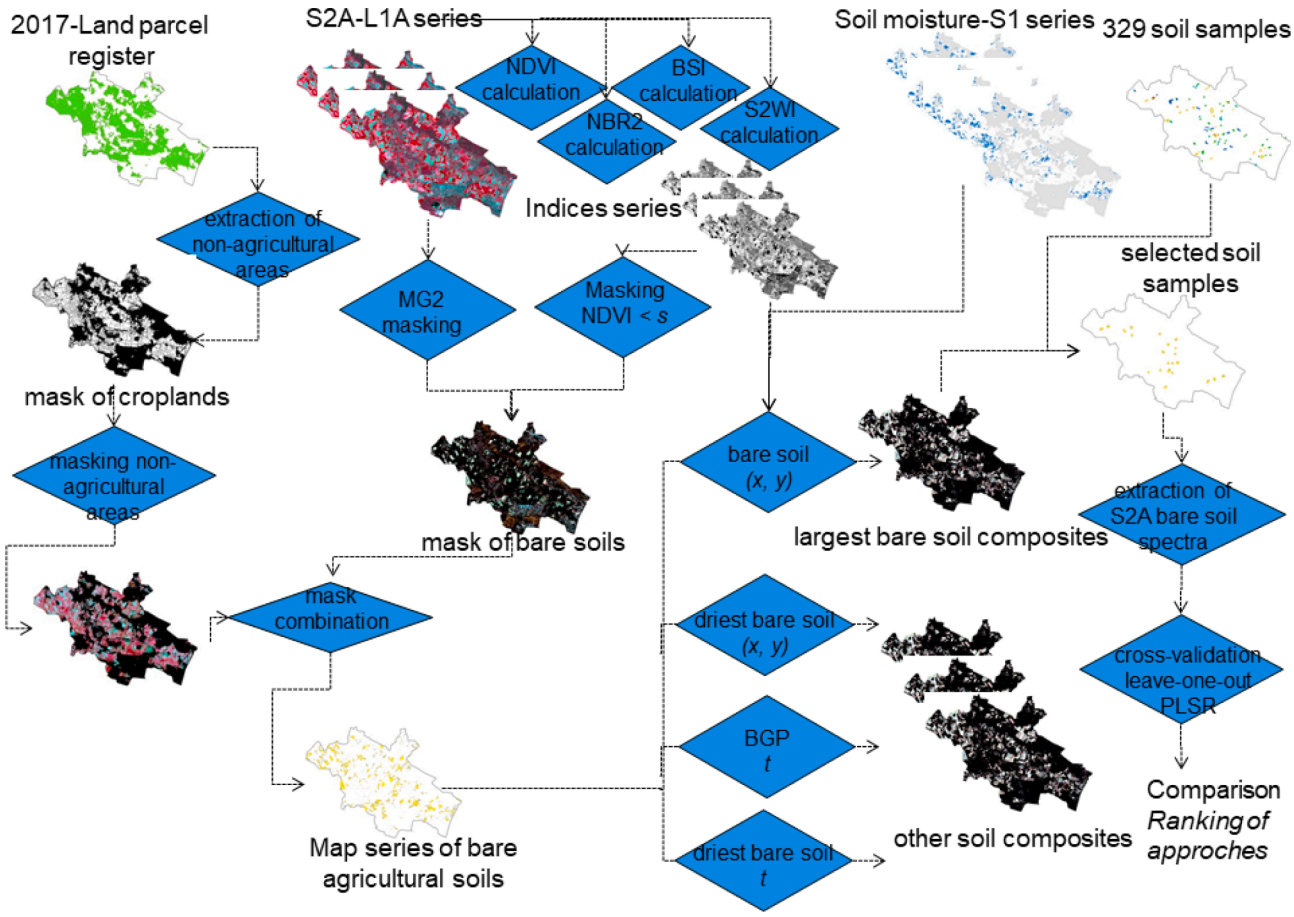

Fig. 3. General flowchart for the mosaicking approach (s = NDVI threshold of either 0.27 or 0.35; BGP = best global performance).

$$NBR2 = \frac{(\rho_{SWIR1} - \rho_{SWIR2})}{(\rho_{SWIR1} + \rho_{SWIR2})} \quad (2)$$

$$BSI = \frac{(\rho_{SWIR2} + \rho_{Red}) - (\rho_{NIR} + \rho_{Blue})}{(\rho_{SWIR2} + \rho_{Red}) + (\rho_{NIR} + \rho_{Blue})} \quad (3)$$

Where ρ is the surface reflectance (%) of the far shortwave infrared (SWIR) (i.e., SWIR1 = B11 band and SWIR2 = B12 band for Sentinel-2), near-infrared (NIR = B8), red and blue spectral regions. Values range between −1 and 1, where a higher NDVI value indicates a higher coverage of chlorophyllian vegetation, while both higher BSI or NBR2 indicate a bare soil without straw.

Driven by the lowest NDVI value amongst a time series. A first bare soil method was based on NDVI and initially designed and used by Loiseau et al. (2019). It requires first choosing a threshold NDVI value for defining a bare soil, in order to discard those pixels with values higher than the chosen threshold, that are assumed to be vegetated. The bare soil pixel at coordinate (x;y) of the date *t* is then kept into the composite image if its NDVI value, i.e. the coverage of photosynthetically active vegetation, is the lowest across the whole time series with the same pixel coordinates (equation (4)).

$$bare\_soil_{(x,y)} = \min_{(t\in[1,T])} NDVI_{(x,y,t)} \text{ AND } NDVI \leq 0.27 \text{ or } 0.35 \quad (4)$$

Where x, y are the geographic coordinates of a given pixel; *t* is the time when the image is acquired across the whole series ranging from 1 to *T* (last date).

This method was initially defined at the national scale of mainland France, for which the harmonized threshold of 0.27 proved to be the best trade-off for getting the highest bare soil area while reducing the effects of sparse vegetation at national scale (Loiseau et al., 2019). In line with this national study, the 0.27 threshold value was tested in this study for NDVI (temporal mosaic named *Bare_soil0.27*, Table 5), but for the remaining methods, the 0.35 threshold value (previously used for this area) was retained for extracting the bare soils (temporal mosaic named *Bare_soil0.35*, Table 5).

The NDVI-based method was applied on the whole series, then on a reduced time series based on the most extended available sequences of bare soil dates for each threshold. For each date, the NDVI image was binarized into bare soil (value 1) and vegetated or cloud or shadow pixel (value 0). Binarized images were stacked and at each pixel, binary values were added, to compute the frequency of bare soil coverage across the 9 dates-series.

In order to characterize the frequency of bare soil coverage into more details, the temporal sequence of binary values was assessed, by adding each binarized NDVI image of a given date multiplied by 10^9 (first date of 12 March 2016) then 10^i (i^{th} date, i comprised between 8 and 1, in decreasing order), to 1 (last date of 19 April 2017). For instance, the "111110000" sequence corresponds to bare soil occurring from 12 March to 27 December 2016 and followed by vegetated pixels for the remaining dates. The most extended sequences of 9 values were therefore identified, and their area calculated.

Driven by the highest BSI value amongst the S2 time-series. The BSI index (equation (2)) used by Diek et al. (2017) with Landsat series at the scale of Switzerland was also tested for extracting the bare soil area at each pixel across the S2 time series (equation (5)).

$$bare\_soilBSI_{(x,y)} = \max_{(t\in[1,T])} BSI_{(x,y,t)} \quad (5)$$

This method was the sole not based on any NDVI threshold, as it was meant to supplant the use of NDVI. The whole series was tested, followed by a reduced time series relying on the quartiles of *maxBSI* values

Table 5
Conditions fulfilled by a pixel from a given date for integrating its reflectance spectrum into the mosaic according to temporal mosaicking methods.

Approach	Driver	Name of temporal mosaic	Way for selections
Per pixel	Bare soil	*Bare_soil 0.27*	NDVI ≤ 0.27 AND minNDVI
Per pixel	Bare soil	*Bare_soil 0.35*	NDVI ≤ 0.35 AND minNDVI
Per pixel	Bare soil	*Bare_soilBSI*	MaxBSI
Per pixel	Bare soil	*Bare_soilNBR2*	NDVI ≤ 0.35 AND GVI1 > 0 AND GVI2 > 0 AND minNBR2
Per pixel	Driest soil	*DriestS2WI_bare_soil*	NDVI ≤ 0.35 AND minS2WI
Per pixel	Driest soil	*DriestS2WI_bare_soilNBR2*	NDVI ≤ 0.35 AND GVI1 > 0 AND GVI2 > 0 AND minNBR2 AND minS2WI
Per pixel	Driest soil	*Driest_bare_soil*	NDVI ≤ 0.35 AND minθ (%vol.)
Per pixel	Driest soil	*Driest_bare_soil, θ < 25%vol.*	NDVI ≤ 0.35 AND minθ (%vol.) < 25%vol.
Per-date	Best date	*BGP*	NDVI ≤ 0.35 AND maxRPD
Per-date	Bare date	*Bare_dateNBR2*	NDVI ≤ 0.35 AND min (meanNBR2)
Per-date	Driest date	*Driest_dateS2WI*	NDVI ≤ 0.35 AND min (meanS2WI)
Per-date	Driest date	*Driest_date$_t$*	NDVI ≤ 0.35 AND min (meanθ(%vol.))
Per-date	Driest date	*Best areal_driest date,* meanθ(% vol.) < 25%vol.	NDVI ≤ 0.35 AND min (meanθ(%vol.)) < 25% vol. AND maxArea
Per-date	Driest date	*Best areal_driest date, meanθ(% vol.)) < 25%vol. NBR2 < 0.09*	NDVI ≤ 0.35 AND min (meanθ(%vol.)) < 25% vol. AND maxArea AND NBR2 < 0.09

amongst the sample set (Table 6).

Driven by the lowest NBR2 value amongst a S2 time-series. The NBR2 index (equation (3)), initially defined by Van Deventer et al. (1997) using the SWIR Landsat TM bands 7 and 5, was later used by Demattê et al. (2018) for extracting the bare soil area at each pixel across a Landsat8 time series in Brazil then adapted for Sentinel-2 by Castaldi et al. (2019b) in Germany. Following these authors, differences between B3 and B2 (green vegetation index GVI1) and B4 and B3 (green vegetation index GVI2) higher than zero (equation (6)) were calculated prior to the NBR2 index (equation (6)).

$$bare\_soilNBR2_{(x,y)} = \min_{(t\in[1,T])} NBR2_{(x,y,t)} \;\; AND \;\; GVI1 > 0 \;\; AND \;\; GVI2 > 0 \quad (6)$$

Prior to this *bare_soilNBR2* method, vegetated pixels were discarded when NDVI value was > 0.35 (Table 5).

The whole S2 series with 9 dates was tested, then reduced time series after discarding the bare soils sample locations having *NBR2* values higher than 3rd quartile, then median, and finally 1st quartile, i.e. keeping the least (or none) dry vegetation cover across the series (Table 6). These threshold values were applied to the min *NBR2* image to calculate the corresponding areas.

2.6.1.2. Driest soil approaches. A second set of per-pixel approaches, named "driest soil approaches", consists in extracting, for a sequence of bare soil pixels, those having the lowest soil water content or likely to be driest according to a soil moisture index. The seek of driest soil is aimed at minimizing the disturbing effects that soil moisture may have on SOC content prediction according to previous studies (Minasny et al., 2011), (Rienzi et al., 2014). Driest soil already includes the use of spectral indices meant to remove either green vegetation (NDVI) or dry vegetation (NBR2), ie selecting bare soil.

Driven by the lowest S2WI value amongst S2 time-series, the '*DriestS2WI_bare_soil*' method relies on the soil moisture index 'S2WI' calculated from S2 images (Vaudour et al., 2019b) as follows (equation (7)):

$$S2WI = \frac{\rho_{(865nm)} - \rho_{(1610nm)} - \rho_{(2190nm)}}{\rho_{(865nm)} + \rho_{(1610nm)} + \rho_{(2190nm)}} \quad (7)$$

Where ρ is surface reflectance (%).

This S2WI index results in negative values for bare soils, ranging from ~ -0.5 to 0 and is useful for separating between very moist (higher values) and very dry soils (lower values) along this time series.

The bare soil pixel at coordinate (x, y) of the date t is kept in this composite image if its S2WI value is the lowest across the whole time series with the same pixel coordinates. Similarly to the bare soil (equation (1)), the driest pixels for each tile are those for which the S2WI value, i.e. an indication of the soil moisture, is minimized across the whole time series for non-masked pixels with the same pixel coordinates (equation (8)).

$$DriestS2WI\_bare\_soil_{(x,y)} = \min_{(t\in[1,T])} S2WI_{(x,y,t)} \;\; AND \;\; NDVI \leq 0.35 \quad (8)$$

Where x ,*y* are the geographic coordinates of a given pixel; t is the time when the image is acquired across the whole series ranging from 1 to T (last date).

For this *DriestS2WI_bare_soil* method, vegetated pixels were discarded when NDVI value was > 0.35. As a matter of fact, when comparing SOC prediction performances for bare soils extracted from threshold values of either 0.27 or 0.35, very similar results were obtained (Vaudour et al., 2019b).

The whole S2 series with 9 dates was tested, then reduced time series after discarding the bare soils sample locations having *minS2WI* values higher than 3rd quartile, then median, and finally 1st quartile, i.e. keeping the driest of the driest soil samples across the series (Table 6). These threshold values were applied to the min S2WI image to calculate the areas covered.

Driven by the lowest S2WI value amongst a S2 time-series for NBR2-derived bare soil, the '*DriestS2WI_bare_soilNBR2*' method relies on the soil moisture index 'S2WI' for bare soil pixels retrieved according to the *Bare_soilNBR2* method, as follows (equation (9)).

$$DriestS2WI\_bare\_soilNBR2_{(x,y)} = \min_{(t\in[1,T])} S2WI_{(x,y,t)} \;\; AND \;\; bare\_soilNBR2_{(x,y,t)} \quad (9)$$

The whole S2 series with 9 dates was tested, then reduced time series after discarding the bare soils sample locations having both *NBR2* and *S2WI* values higher than 3rd quartile each, then median (1st quartile not retained because of insufficient sample size), i.e. keeping both least (or none) dry vegetation cover and driest soils across the series. The areas covered were obtained by crossing the quartile classified images of both NBR2 and S2WI.

Driven by the lowest S1-estimated soil moisture amongst a time-series, the "*driest bare soil*' method relies on minimizing the S1-derived soil

Table 6
Indices statistics for the largest sample sets available. Skewness is of type 3 according to Joanes and Gill (1998).

Index	Number of samples	Min	1st quartile	median	mean	3rd quartile	Max	Standard deviation	skewness
max BSI across 9 dates	329	−0.545	0.026	0.134	0.081	0.188	0.299	0.176	−1.9
min NBR2 across 9 dates	299	0.02	0.053	0.088	0.112	0.159	0.358	0.05	0.7
min S2WI across 9 dates	261	−0.53	−0.44	−0.41	−0.40	−0.36	−0.17	0.06	0.7

moisture content θ for bare soils, according to the NDVI-threshold of 0.35, amongst the 9 dates (equation (10)).

$$Driest\_bare\_soil_{(x,y)} = \min_{(t\in[1,T])} \theta_{(x,y,t)} \;\; AND \;\; NDVI \leq 0.35 \quad (10)$$

Because of limited sample size, only one reduced time series relying on the pixels the min θ was lower than 25% vol. was tested. The threshold value of 25%vol. was applied to the min θ image to calculate the area covered.

2.6.2. Per-date approaches

Per-date approaches rely on the ranking of images according to an average or global indicator. They were tested on the whole series, then on reduced series removing one date each time. The area reached by each mosaic was computed by adding successively the bare soil pixels of a given date that were not already included from the previous date, through conditional requests. This set of approaches implies that a significant part of each mosaic will contain pixels originating from a same date, while a minority of pixels will be retained from other dates according to their ranking.

Driven by the highest global performance value amongst a time series, the "*best date*" mosaicking consists of ranking the best global performance for each date, according to the RPD value of a given date (Vaudour et al., 2019b, Table 4). The bare soil pixel of the tile *t* remains in the composite image if the prediction performance obtained for the single tile *t* is the best one across the whole time series (BGP, equation (11)).

$$BGP_t = \max_{(t\in[1,T])} RPD_{(t)} \;\; AND \;\; NDVI \leq 0.35 \quad (11)$$

For this performance-based mosaicking, vegetated pixels were discarded when NDVI value was > 0.35; the same as for the other per-date mosaics.

Driven by the NBR2-based bare image amongst a time series, the "*bare date*" mosaicking consists of ranking by date the average NBR2 index computed for bare soils (equation (12)).

$$Bare\_dateNBR2_t = \min_{(t\in[1,T])} (meanNBR2)_t \;\; AND \;\; NDVI \leq 0.35 \quad (12)$$

Driven by the S2WI-based driest image amongst a time series, the "*driest dateS2WI*" mosaicking consists of ranking by date the average soil water index computed for bare soils (equation (13)).

$$Driest\_dateS2WI_t = \min_{(t\in[1,T])} (meanS2WI)_t \;\; AND \;\; NDVI \leq 0.35 \quad (13)$$

Driven by the S1-derived soil water content amongst a time series, the approach selecting the driest image, or "*driest date*" mosaicking, consists of ranking by date the average S1-derived soil water content computed for bare soils (Table 3) (equation (14)).

$$Driest\_date_t = \min_{(t\in[1,T])} (mean\theta)_t \;\; AND \;\; NDVI \leq 0.35 \quad (14)$$

The main purpose of mosaicking is to extend the predicted area. To comply with such purpose the spatial extent covered shall be taken into account when adding a date. Considering that only soil water content higher than 25% will have a dramatic effect on prediction performance (Rienzi et al., 2014), a variant of this driest date method named «*areal/driest date compromise*» consists of discarding the dates with mean water content ≥ 25% and then ordering the dates by increasing mean water content θ, and for two dates with values of θ differing by<6%, selecting the date covering the largest area.

3. Results

Mosaicking approaches were analysed according to i) their performances of SOC content prediction and ii) the total area on which predictions could be performed.

3.1. Maximum bare area mapped across the time series

Globally, using a NDVI threshold of 0.27, slightly more than half of the area (51.9%) was never detected as bare soil across the time series, while such no detection dropped to as low as 36.7% for a 0.35 value, i.e. 63.3% of the agricultural area was detected as bare across the whole 9-dates time series (Table 7). Whatever threshold, the frequency of bare soil detection ranged from 0 to 9 times, but with a very low occurrence for>5 times (Table 7).

For the 0.35-threshold, the bare soil coverage of the agricultural area varied from 8 to 49% amongst dates, being generally close to 16% in late Spring (Fig. 4). About half of the bare soils were detected either once (16.5 km^2) or twice (15.3 km^2), while the remaining were detected three times or up to 8 (10 to 15% additional area each) or even 9 times (~6% additional area) (Fig. 5).

For NDVI ≤ 0.35, over the whole time series, about a hundred binary sequences of bare/non bare soil were observed, amongst which ten only covered>1 km^2 each (Table 8). The most extended sequence was the 4-dates "110110000" sequence of bare soil in March, then November and December 2016 (>5 km^2), followed by the 6 dates "000111111" sequence of bare soil from November 2016 to April 2017 (3.8 km^2).

3.2. Composition and spatial distribution of the samples gathered for each mosaic

The sample sizes resulting from the selection process for each mosaic were comprised between 40 and 329 and 143 and 268 for the per-pixel approaches (Table 9) and per-date approaches (Table 10) respectively. Distributions of SOC contents were slightly positively skewed whatever sample set (type 3 skewness according to Joanes and Gill (1998)), but normal according to D'Agostino, Shapiro-Wilks, Cramer von Mises and Anderson-Darling normality tests (Wuertz et al., 2020).

For most samples, SOC contents values ranged between 6 and 8 and 32–36 $g.kg^{-1}$, were around 14–15 $g.kg^{-1}$ in average with a standard deviation of ~ 5 $g.kg^{-1}$. This holds particularly true for per-dates approaches (Table 10), suggesting that mosaic samples were very similar to the whole sample set, and homogeneously spread over the area.

However, the smallest samples of per-pixel approaches were specific samples, with lower mean and tighter range compared to the others.

3.3. Performances of per_pixel mosaics

Most of PLSR models based on per-pixel mosaics constructed from minimizing or maximizing a spectral index value per pixel yielded poor performances ($R^2_{cv} \leq 0.3$, $RPD_{cv} \leq 1.2$, RPIQ < 1.7, Table 11), whatever the number of dates incorporated. Only models based on 3 mosaics provided suitable SOC prediction performances: the *DriestS2WI_bare_soilNBR2* mosaic, obtained with indices values lower than the median for both indices, the *Bare_soilNBR2* mosaic obtained with indices values lower than the 1st quartile (0.053)) and the *Driest bare soil* mosaic, obtained with θ < 25% vol.. These 3 best performing approaches incorporated less dates (4 dates only for the *DriestS2WI_bare_soilNBR2* and *Bare_soilNBR2* mosaics) and relied on small datasets (around 40 samples for the highest RPD values obtained with the *Driest bare soil* mosaic, with θ < 25% vol) (Table 11).

According to our previous analysis of the SOC prediction performances (Vaudour et al., 2019b), poor results can be explained by the composition of the dates incorporated into mosaics (Fig. 6&7), which is dominated by dates characterized by disturbing factors such high soil moisture (ie., Spring date of 12 March 2016) and both high soil moisture and surface roughness (30 November 2016, 27 December 2016). These dates did not enable sufficient individual performances, having RPD values below 1.2 (Table 4). For the per-pixel approaches, such poorly predictive dates remain predominant for the NDVI-based Bare-soil even when 4 dates only compose a mosaic (Fig. 7), and remain well represented for *DriestS2WI_bare_soil* and *Bare_soilBSI*.

Table 7
Proportion of bare soil detected and detection frequency among 9 dates according to NDVI threshold. Detection frequency range from 0 (never detected) to 9 (always detected).

	Number of times bare soil was detected among the *9* dates										
	NDVI	0	1	2	3	4	5	6	7	8	9
% of pixels detected	<0.27	51.9 (55.1)	13.0 (13.8)	9.5 (10.1)	6.8 (7.2)	7.6 (8.0)	6.4 (6.8)	3.3 (3.5)	0.7 (0.8)	0.5 (0.6)	0.3 (0.3)
(area detected km^2)	<0.35	36.7 (38.9)	16.5 (17.5)	15.3 (16.2)	7.0 (7.4)	8.1 (8.6)	9.2 (9.8)	4.8 (5.1)	1.1 (1.2)	0.9 (1.0)	0.4 (0.4)

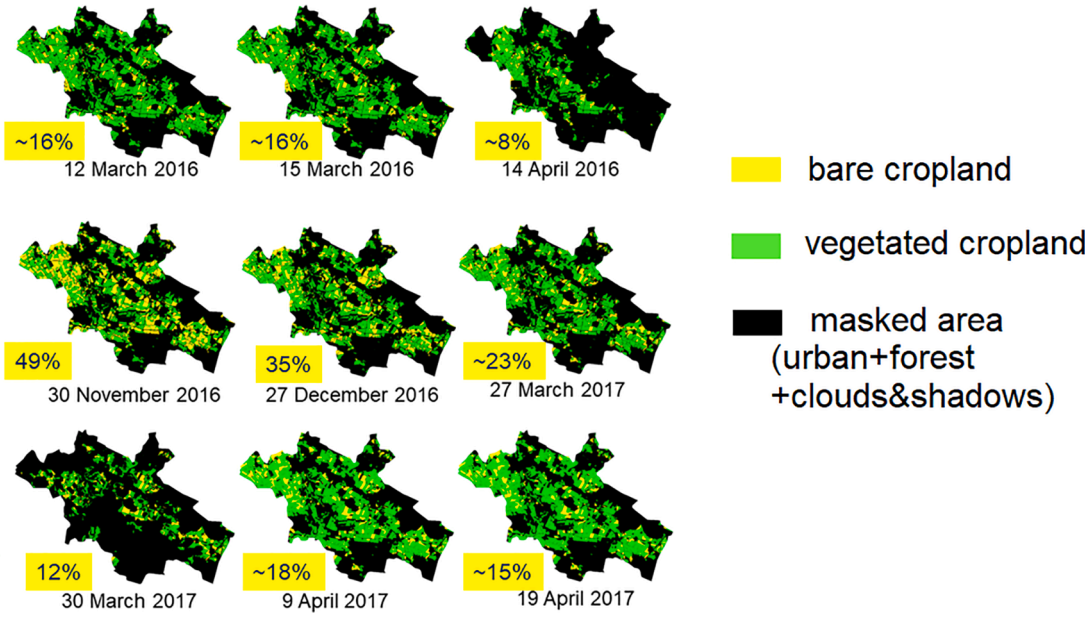

Fig. 4. Map of the percentage of bare soil coverage for the agricultural area according to acquisition date (NDVI ≤ 0.35).

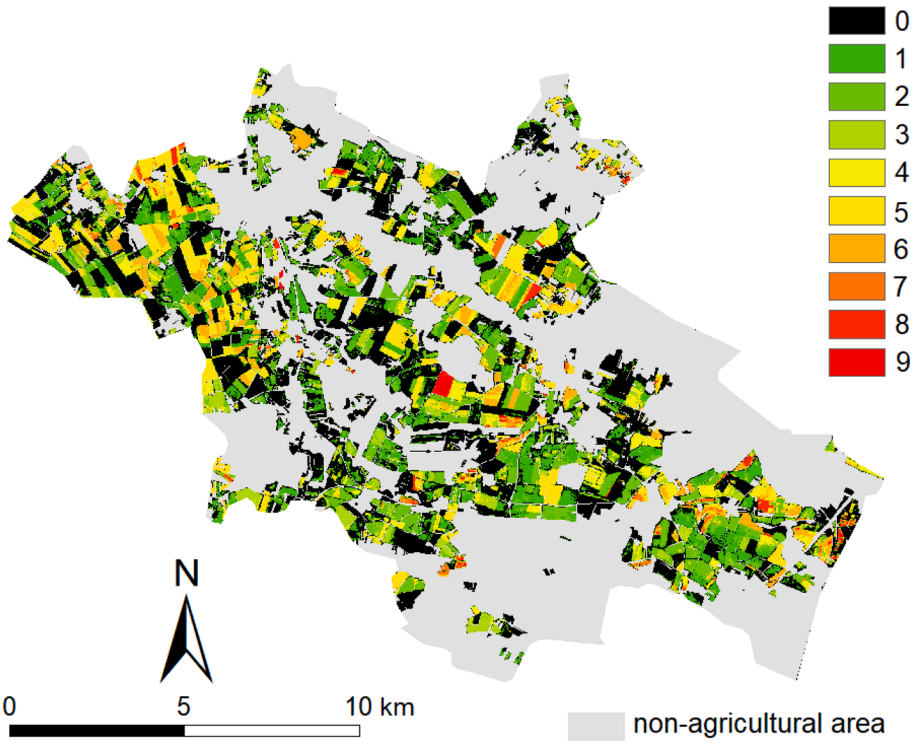

Fig. 5. Map of the frequency of bare soil detection for the agricultural area over the whole time series (NDVI ≤ 0.35).

Table 8
Most extended sequences of detected bare soil.

Sequence	Number of dates	area (km^2) for NDVI ≤ 0.27	area (km^2) for NDVI ≤ 0.35
000100000, bare soil in Dec16	1	10.52	14.76
000110000, bare soil in Dec16 + beginning of March17	2	3.68	10.75
110000000, bare soil in March16	2	3.30	2.44
110100000, bare soil in March + Nov16	3	1.63	1.51
111000000, bare soil in March + Apr16	3	1.35	1.39
110110000, bare soil in March + Nov + Dec16	4	2.68	5.15
111100000, bare soil from March to Nov16	4	2.02	1.14
111110000, bare soil from March to Dec16	5	0.89	2.66
000011111, bare soil from Dec16 to Apr17	5	1.52	1.51
000111111, bare soil from Nov16 to Apr17	6	2.59	3.84

While obtained from a reduced dataset, the best predicting per-pixel approaches suggest that driest soils enable to better predict SOC contents. The 4 dates- *DriestS2WI_bare_soilNBR2* mosaic exhibits some synergy between the soil moisture index S2WI and the bare soil index NBR2, but this mosaic obtained from minimizing two indices (minS2WI, ≤-0.41, minNBR2 ≤ 0.087) relied on a very low sample size (40), and covered a small extent while the NBR2-derived mosaic with values lower than 0.05 covered<1/10 of the agricultural area. The 7 dates- *Driest bare soil* mosaic for θ < 25% vol. provided a high RPDcv showing an artificially good performance that is contradicted by a low RPIQcv, presumably because of higher skewness and limited spread of values.

Finally, none of these per-pixel mosaics with acceptable performance covered an area higher than the individual images yielding comparable performance (Table 4). While the date of 19 April 2017 was predominant in their composition (Fig. 6&7), none of these approaches yielded higher performance than that obtained from this best single date of 19 April 2017 (RPD_{cv} = 1.54, Table 4).

3.4. Performances of per_date mosaics

Overall, compared to per pixel-mosaics based on the whole time series, a higher number of mosaics constructed from minimizing a spectral index value per date yielded acceptable performance, with 3 dates at least (Table 12). The best performance was reached for the *Driest_date* approach with 3 dates (RPDcv of 1.50), followed by the *Best_areal_Driest_date* compromises with 4 dates (RPDcv of 1.43) and 4 dates plus NBR2 ≤ 0.09 (RPDcv of 1.47), the *Bare_dateNBR2* with 3 dates (RPDcv of 1.46), and finally the *BGP* with 3 or 4 dates (RPDcv of 1.43 and 1.41, respectively). Yet the performance of the mosaic constructed from 5 dates based on the *BGP* approach was still close to fair. Of these best models, the 4-dates *Best_areal_Driest_date* compromises and the 4 dates-BGP had acceptable RPIQcv value comprised between 1.8 and 2.0 for both cross-validation (Table 12) and validation (Table 13).

As observed for the per-pixel mosaics, and for the same reasons (Fig. 8), using the whole series resulted in poor performances.

The *Best_areal_Driest_date* mosaic with 4 dates enables the most extended predicted area, covering nearly 60% of the largest NDVI-based bare soil predictable area (Table 7). While the size of the contributing sample (180) was very close to that of BGP obtained with 4 dates (187), the spatial distribution of the contributing fields was more evenly spread over the study area, with greater areal contribution of the third and fourth dates incorporated (Fig. 9).

The aerial gain enabled by the best mosaics (Table 7) was more than twofold that of the single image of 19 April 2017 (Table 4), which was not only the first image standing out in their composition, but also the one giving rise to the best single-date performance (RPDcv of 1.54, Table 4). The spatial patterns of the best 4-dates mosaics were very similar (Fig. 10), with a median value of the residual of SOC content prediction slightly lower for the *Best_areal_Driest_date* mosaic (Fig. 11).

The above-mentioned best models suggest that it is not advisable to add>4 dates if one wishes to maintain an acceptable SOC prediction performance. The more the pixels heterogeneity due to date is limited,

Table 9
Statistics of soil organic carbon (SOC) contents (g.kg–1) according to per-pixel mosaics. Please refer to Table 6 for the meaning of the chosen thresholds. N, number of calibration samples; *q1*; first quartile; μ, mean; *q3*; third quartile; σ, standard deviation; Sk, skewness.

Mosaic	N	min	*q1*	μ	*q3*	max	σ	Sk
Bare_soil, NDVI ≤ 0.27	239	6.20	11.40	15.45	18.30	35.90	5.20	1.14
Bare_soil, NDVI ≤ 0.27, 000,111,111	167	6.20	11.40	15.01	17.45	35.90	5.25	1.51
Bare_soil, NDVI ≤ 0.27, 000,011,111	134	6.20	11.60	15.43	18.98	28.40	4.74	0.56
Bare_soil, NDVI ≤ 0.27, 111,100,000	131	6.20	11.60	15.40	18.55	28.40	4.73	0.61
Bare_soil, NDVI ≤ 0.27, 110,100,000	118	6.20	11.80	15.55	18.98	28.40	4.84	0.55
Bare_soil, NDVI ≤ 0.35	271	6.20	11.40	15.44	18.45	35.90	5.29	1.04
Bare_soil, NDVI ≤ 0.35, 000,111,111	193	6.20	11.10	15.04	17.80	35.90	5.40	1.33
Bare_soil, NDVI ≤ 0.35, 111,110,000	164	6.20	11.45	15.38	19.30	29.10	4.96	0.57
Bare_soil, NDVI ≤ 0.35, 110,110,000	157	6.20	11.30	15.32	19.10	29.10	4.99	0.61
Bare_soil, NDVI ≤ 0.35, 110,100,000	144	6.20	11.20	15.43	19.30	29.10	5.10	0.56
Bare_soilBSI	329	6.20	11.28	15.42	18.50	35.90	5.23	0.97
Bare_soilBSI, >0.027	245	6.20	11.40	15.49	18.30	35.90	5.23	1.14
Bare_soilBSI, >0.134	164	8.92	11.40	15.11	17.73	35.00	4.66	1.21
Bare_soilBSI, >0.188	83	9.06	11.40	14.98	17.90	31.90	4.27	1.09
Bare_soilNBR2	299	6.38	11.10	15.40	18.50	35.90	5.29	1.00
Bare_soilNBR2, ≤0.159	245	7.04	11.40	15.35	18.30	35.90	5.18	1.18
Bare_soilNBR2, ≤0.087	163	7.04	11.40	15.19	18.15	31.90	4.72	0.87
Bare_soilNBR2, ≤0.053	81	8.92	10.50	13.73	16.20	26.60	3.80	0.96
DriestS2WI_bare_soil	261	6.20	11.40	15.57	18.50	35.90	5.33	1.01
DriestS2WI_bare_soil, ≤-0.36	198	7.04	11.40	15.52	18.30	35.90	5.39	1.24
DriestS2WI_bare_soil, ≤-0.41	138	8.92	11.40	15.86	19.60	35.00	5.36	0.99
DriestS2WI_bare_soil, ≤-0.44	81	9.13	12.10	15.92	19.30	31.90	4.81	0.84
DriestS2WI_bare_soilNBR2	143	7.04	11.40	15.44	18.50	35.90	5.65	1.23
DriestS2WI_bare_soilNBR2, minS2WI, ≤-0.36, minNBR2 ≤ 0.159	83	7.04	11.40	14.92	15.85	35.90	5.80	1.78
DriestS2WI_bare_soilNBR2, minS2WI, ≤-0.41, minNBR2 ≤ 0.087	40	9.04	11.40	14.23	16.32	24.60	3.87	0.95
Driest_bare_soil	84	8.09	11.00	15.18	18.07	31.90	5.82	1.14
Driest bare soil, , θ < 25%vol.	42	8.92	10.35	14.17	14.80	31.90	5.63	1.62

Table 10
Statistics of soil organic carbon (SOC) contents (g.kg–1) according to per-date mosaics. N, number of calibration samples; *q1*; first quartile; μ, mean; *q3*; third quartile; σ, standard deviation; Sk, skewness.

Mosaic, NDVI ≤ 0.35	Number of dates included *t*	N	min	*q1*	μ	*q3*	max	σ	Sk
BGP_t	9	268	6.20	11.40	15.48	18.50	35.90	5.31	1.03
BGP_t	8	241	6.20	11.40	15.53	18.50	35.90	5.28	1.05
BGP_t	7	237	6.20	11.40	15.45	18.30	35.90	5.29	1.09
BGP_t	6	235	6.20	11.40	15.46	18.30	35.90	5.30	1.10
BGP_t	5	198	6.38	11.43	15.64	18.38	35.90	5.35	1.14
BGP_t	4	187	6.38	11.40	15.77	18.50	35.90	5.44	1.08
BGP_t	3	173	6.38	11.40	15.08	18.00	31.90	4.72	0.86
Bare_dateNBR2	7	268	6.20	11.40	15.48	18.50	35.90	5.31	1.03
Bare_dateNBR2	6	203	6.38	11.45	15.71	18.85	35.90	5.34	1.08
Bare_dateNBR2	5	201	6.38	11.50	15.72	18.60	35.90	5.35	1.09
Bare_dateNBR2	4	197	6.38	11.40	15.64	18.40	35.90	5.36	1.14
Bare_dateNBR2	3	173	6.38	11.40	15.08	18.00	31.90	4.72	0.86
Driest_dateS2WI	6	268	6.20	11.40	15.48	18.50	35.90	4.77	1.03
Driest_dateS2WI	5	266	6.20	11.40	15.44	18.38	35.90	5.31	1.05
Driest_dateS2WI	4	199	6.38	11.40	15.63	18.45	35.90	5.36	1.13
Driest_dateS2WI	3	198	6.38	11.43	15.66	18.48	35.90	5.36	1.12
Driest_date	9	268	6.20	11.40	15.48	18.50	35.90	5.31	1.03
Driest_date	8	241	6.20	11.40	15.53	18.50	35.90	5.28	1.05
Driest_date	7	204	6.38	11.47	15.71	18.73	35.90	5.33	1.08
Driest_date	6	202	6.38	11.50	15.72	18.57	35.90	5.33	1.09
Driest_date	5	184	6.38	11.57	15.72	18.50	35.90	5.34	1.16
Driest_date	4	172	6.38	11.68	15.87	18.73	35.90	5.45	1.10
Driest_date	3	143	6.38	11.55	15.87	18.40	35.90	5.56	1.21
Areal_driest_date compromise, θ ≤ 25%, NBR2 ≤ 0.09	4	157	6.36	11.40	15.64	18.40	35.90	5.36	0.84
Best areal_driest_date compromise, θ < 25%	4	180	6.38	11.47	15.71	18.43	35.90	5.34	1.18
Common calibration dataset	4	105	6.38	11.55	15.90	18.40	35.90	5.62	1.23
Common validation dataset	4	51	8.92	11.60	15.71	18.40	31.90	5.21	1.00

Table 11
Cross-validation performances of per-pixel-based mosaics and their spatial coverages (For Bare_soil, the most represented rotations are described by a succession of 0 (vegetated soil, not used in the mosaic) and 1 (bare soil) for each of the 9 dates starting from 12 March 2016 on the left). Nd, number of dates included; N, number of samples; N_{LV}, number of latent variables.

Mosaic	Nd	N	N_{LV}	$RMSE_{cv}$ (g.kg^{-1})	R^2_{cv}	RPD_{cv}	$RPIQ_{cv}$	Area covered (km^2)
Bare_soil, NDVI ≤ 0.27	9	239	3	4.90	0.11	1.06	1.41	50.96
Bare_soil, NDVI ≤ 0.27, 000,111,111	6	167	6	5.00	0.09	1.05	1.21	25.85
Bare_soil, NDVI ≤ 0.27, 000,011,111	5	134	4	4.60	0.05	1.03	1.60	15.2
Bare_soil, NDVI ≤ 0.27, 111,100,000	4	131	4	4.17	0.22	1.13	1.67	20.2
Bare_soil, NDVI ≤ 0.27, 110,100,000	3	118	5	4.18	0.25	1.16	1.72	16.3
Bare_soil, NDVI ≤ 0.35	9	272	3	5.15	0.05	1.03	1.37	67.13
Bare_soil, NDVI ≤ 0.35, 000,111,111	6	193	6	5.20	0.07	1.04	1.29	38.4
Bare_soil, NDVI ≤ 0.35, 111,110,000	5	164	6	5.00	−0.02	0.99	1.57	26.6
Bare_soil, NDVI ≤ 0.35, 110,110,000	4	157	5	4.34	0.24	1.15	1.80	51.49
Bare_soil, NDVI ≤ 0.35, 110,100,000	3	144	5	4.36	0.27	1.17	1.86	15.07
Bare_soilBSI	9	329	5	4.85	0.14	1.08	1.49	106.06
Bare_soilBSI, >0.02699	8	245	4	4.75	0.17	1.10	1.45	53.81
Bare_soilBSI, >0.13359	7	164	6	4.23	0.17	1.10	1.50	28.05
Bare_soilBSI, >0.18767	5	83	5	3.43	0.35	1.24	1.90	10.96
Bare_soilNBR2	8	299	4	4.72	0.20	1.12	1.57	99.17
Bare_soilNBR2, ≤0.159	8	245	4	4.56	0.22	1.13	1.51	55.94
Bare_soilNBR2, ≤0.087	7	163	4	3.51	0.44	1.34	1.92	28.12
Bare_soilNBR2, ≤0.053	4	81	4	2.67	0.50	**1.42**	2.13	9.31
DriestS2WI_bare_soil	8	261	6	5.10	0.08	1.04	1.39	66.45
DriestS2WI_bare_soil, ≤-0.36	6	198	3	5.11	0.10	1.05	1.35	38.00
DriestS2WI_bare_soil, ≤-0.41	6	138	3	5.02	0.12	1.07	1.63	20.76
DriestS2WI_bare_soil, ≤-0.44	5	81	3	3.97	0.32	1.21	1.81	10.26
DriestS2WI_bare_soilNBR2	6	143	5	5.22	0.14	1.08	1.36	66.45
DriestS2WI_bare_soilNBR2, minS2WI, ≤-0.36, minNBR2 ≤ 0.159	5	83	3	5.45	0.11	1.06	0.82	37.14
DriestS2WI_bare_soilNBR2, minS2WI, ≤-0.41, minNBR2 ≤ 0.087	4	40	4	2.53	0.56	**1.53**	1.94	**16.69**
Driest_bare_soil	8	84	4	5.01	0.25	1.16	1.41	28.91
Driest bare soil, θ < 25%vol.	7	42	8	3.74	0.55	**1.51**	1.19	15.97

the better is prediction performance. When examining the residuals of 4 dates-mosaics (Fig. 12), the dates of 19 April 2017, and in a lesser degree, 9 April 2017, are those giving rise to the lowest residuals, followed by 15 March 16, and then 27 and 30 March 2017 (less performing dates).

None of the multidate models reached a performance as high as the single date of 17 April 2017, i.e. multidate mosaics enabled to increase, and more than double, the predicted area but not the prediction performance compared to the best single date. Benefiting volumetric soil moisture information derived from S1 contributed to the most efficient strategy for reaching the best areal compromise whilst maintaining acceptable performance. Whatever approach, the best models are models retaining the driest soil conditions.

4. Discussion

Single date acquisitions hardly enable to derive SOC prediction over

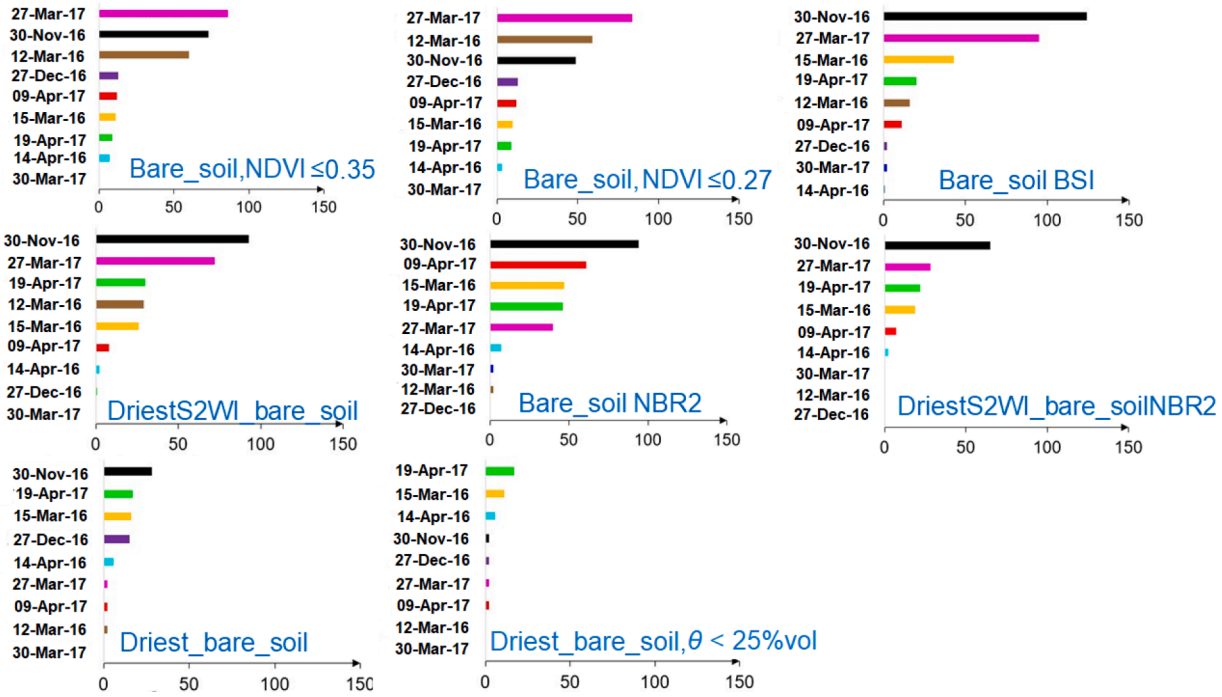

Fig. 6. Composition of per-pixel mosaics starting from the maximum possible dates (the x-axis is the number of soil samples selected from a given method).

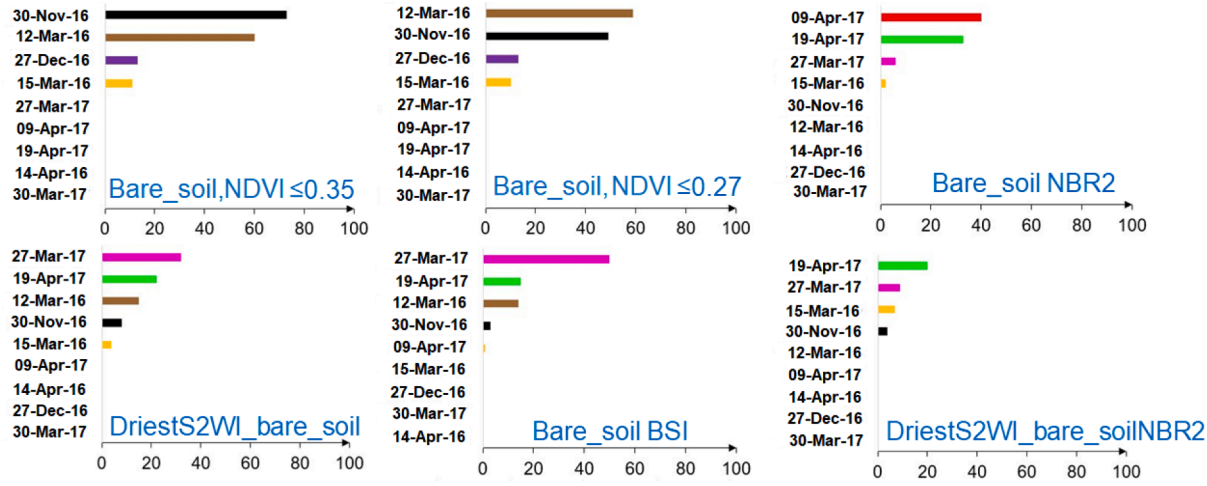

Fig. 7. Composition of per-pixel mosaics obtained from 4 or 5 dates (the x-axis is the number of soil samples selected from a given method).

a sufficient percentage of the agricultural area. This study shows that a limited period of two years enables to construct multidate mosaics to widen the bare soil coverage within a cropland area characterized by 3 or 4 years-rotations, while maintaining acceptable SOC prediction performance, but this highly depends on the choice of the mosaicking approach as well as the selection of dates included.

4.1. *Per-pixel approaches for mosaicking*

Whatever approach used for creating a per-pixel mosaic, the predicted SOC maps obtained from these mosaics remain less accurate than the one produced using the single-date S2 data acquired on 19 April 2017 (RPDcv = 1,54 and 16.24 km^2, Table 4, Vaudour et al., 2019a,b). Some of them are even less extended following one or several thresholding steps, which limit the number of composing pixels fulfilling the pertaining conditions.

Composites created by per-pixel approaches focused on bare soil extraction (e.g. Diek et al., 2017; Rogge et al., 2018; Gallo et al., 2018; Demattê et al., 2018, Loiseau et al., 2019) were based on available bare soil pixels from different images acquired at different dates. Pixels in this kind of composite are collected at different dates, resulting in between pixels-variations in soil surface conditions such as soil moisture and soil surface roughness. For instance, over the Versailles Plain, soil surface roughness expressed through the root mean square surface height *Hrms* varied between 0.7 and 3.5 cm (Vaudour et al., 2014b, 2019b; Baghdadi et al., 2018), the spatial variations of which were due to tillage operations, and the between-dates variations marked by narrower histogram of values in Spring with lower *Hrms* values than in Autumn and Winter (Vaudour et al., 2019b). None of the mosaics obtained from a per-pixel approach driven only by the NDVI vegetation index allowed an acceptable SOC prediction performance, whatever the number of included dates and the chosen threshold for NDVI value (Table 11). Thus, even though the soil remote sensing community widely uses NDVI to extract bare soil in single-date images prior to modelling soil surface

Table 12
Cross-validation performances of per-date mosaics and their spatial coverages. Nd, number of dates included; N, number of samples; N_{LV}, number of latent variables.

Mosaic, NDVI ≤ 0.35	Nd	N	N_{LV}	$RMSE_{cv}$ (g.kg^{-1})	R^2_{cv}	RPD_{cv}	$RPIQ_{cv}$	Area covered (km^2)
BGP	9	268	4	4.36	0.32	1.22	1.63	67.13
BGP	8	241	4	4.28	0.34	1.23	1.66	52.37
BGP	7	237	4	4.31	0.33	1.23	1.60	51.85
BGP	6	235	4	4.28	0.34	1.24	1.61	50.93
BGP	5	198	6	3.87	0.48	**1.38**	1.80	39.73
BGP	4	187	6	3.85	0.50	**1.41**	1.84	36.47
BGP	3	173	6	3.30	0.51	**1.43**	2.00	34.34
Bare_dateNBR2	7	268	5	4.64	0.23	1.14	1.53	66.66
Bare_dateNBR2	6	203	3	4.23	0.37	1.26	1.75	41.34
Bare_dateNBR2	5	201	3	4.13	0.40	1.29	1.72	40.29
Bare_dateNBR2	4	197	3	4.16	0.40	1.29	1.68	39.68
Bare_dateNBR2	3	173	6	3.24	0.53	**1.46**	2.04	34.28
Driest_dateS2WI	6	268	4	4.77	0.19	1.11	1.49	66.76
Driest_dateS2WI	5	266	6	4.73	0.20	1.12	1.48	66.41
Driest_dateS2WI	4	199	4	4.77	0.21	1.12	1.48	40.61
Driest_dateS2WI	3	198	4	4.76	0.21	1.13	1.48	38.49
Driest_date	9	268	4	4.63	0.24	1.15	1.53	67.13
Driest_date	8	267	4	4.63	0.24	1.15	1.52	66.43
Driest_date	7	239	5	4.52	0.27	1.17	1.57	51.49
Driest_date	6	202	5	3.98	0.44	1.34	1.78	40.32
Driest_date	5	201	5	3.98	0.44	1.34	1.78	40.18
Driest_date	4	197	5	4.02	0.44	1.34	1.79	39.59
Driest_date	3	154	5	3.62	0.55	**1.50**	1.88	25.86
Areal_driest_date compromise, θ ≤ 25%, NBR2 ≤ 0.09	4	157	6	3.26	0.54	**1.47**	2.15	22.47
Best areal_driest_date compromise, θ < 25%	4	180	6	3.74	0.51	**1.43**	1.86	**39.67**

Table 13
Validation performances of four-date mosaics for a common dataset. Nb_{cal} - Nb_{val} refers to the number of calibration and validation samples, respectively. N_{LV}, number of latent variables.

Mosaic, NDVI ≤ 0.35	Nbcal - Nbval	N_{LV}	$RMSE_{cal}$ (g. kg^{-1})	R^2_{cal}	RPD_{cal}	$RPIQ_{cal}$	$RMSE_{val}$ (g. kg^{-1})	R^2_{val}	RPD_{val}	$RPIQ_{val}$
BGP	103–51	5	4.14	0.45	**1.36**	1.65	3.56	0.52	**1.46**	1.91
Bare_dateNBR2	103–51	5	4.35	0.40	1.29	1.57	3.94	0.42	1.32	1.73
Driest_dateS2WI	103–51	6	5.47	0.04	1.03	1.25	4.36	0.28	1.19	1.56
Driest_date	103–51	4	4.08	0.47	**1.38**	1.68	4.22	0.33	1.23	1.61
Best areal_driest_date compromise, θ ≤ 25%, NBR2 ≤ 0.09	89–43	5	3.42	0.42	**1.43**	2.02	3.30	0.54	**1.37**	2.09
Best areal_driest_date compromise, θ ≤ 25%	103–51	6	3.90	0.51	**1.38**	1.76	3.72	0.48	**1.40**	1.83

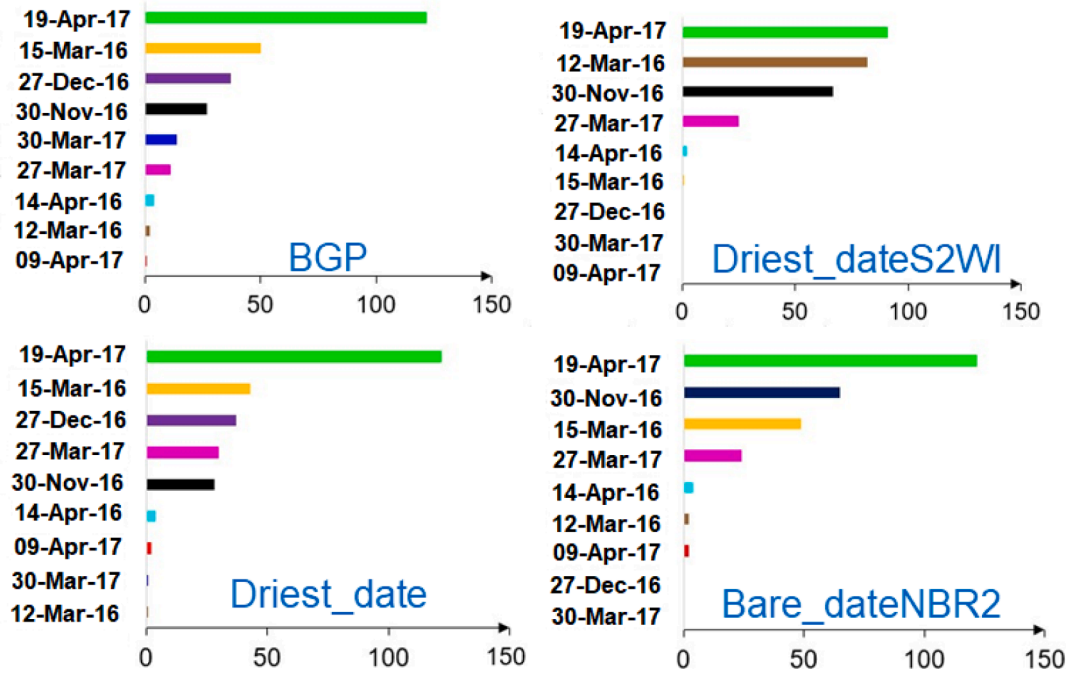

Fig. 8. Composition of per-date mosaics from the maximum number of available dates (the x-axis is the number of soil samples selected from a given method).

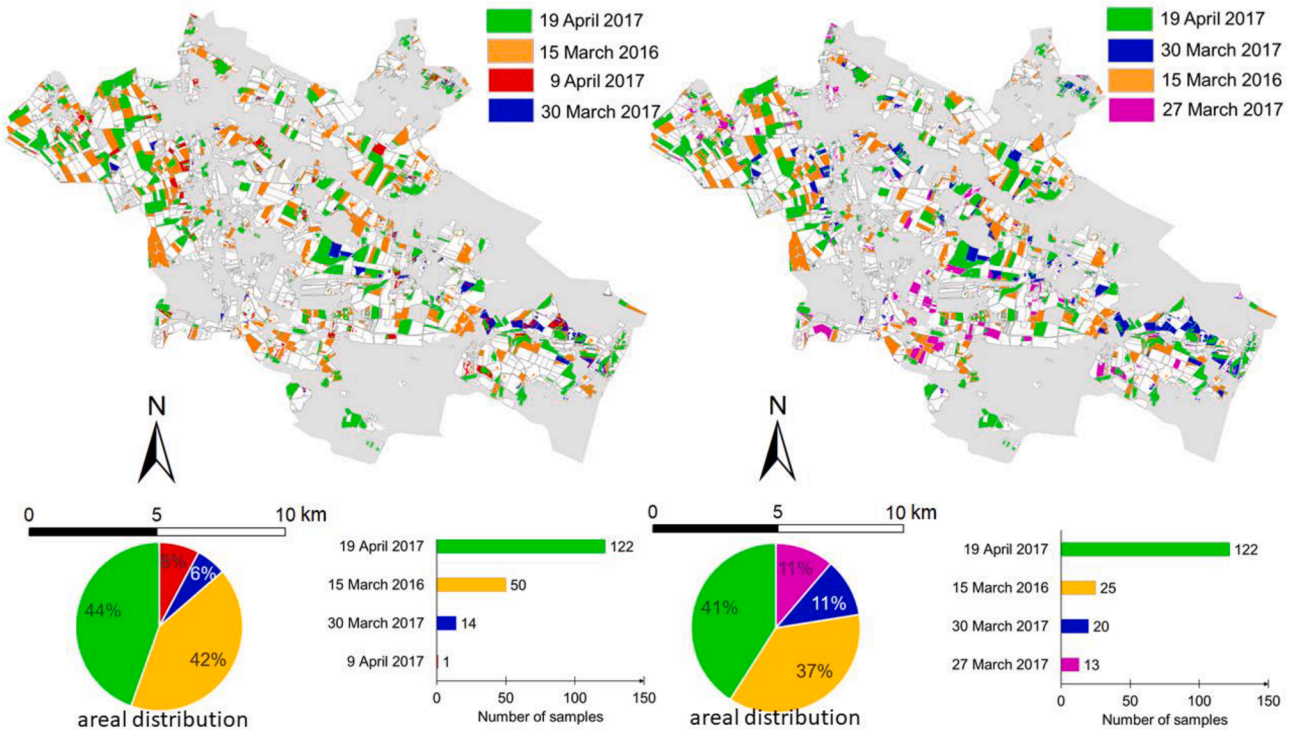

Fig. 9. Spatial distribution and composition of the best per-date mosaics obtained from 4 dates (left, *BGP*; right, *Best areal_driest_date* trade-off; grey areas are non-agricultural areas, white areas are unpredicted vegetated fields).

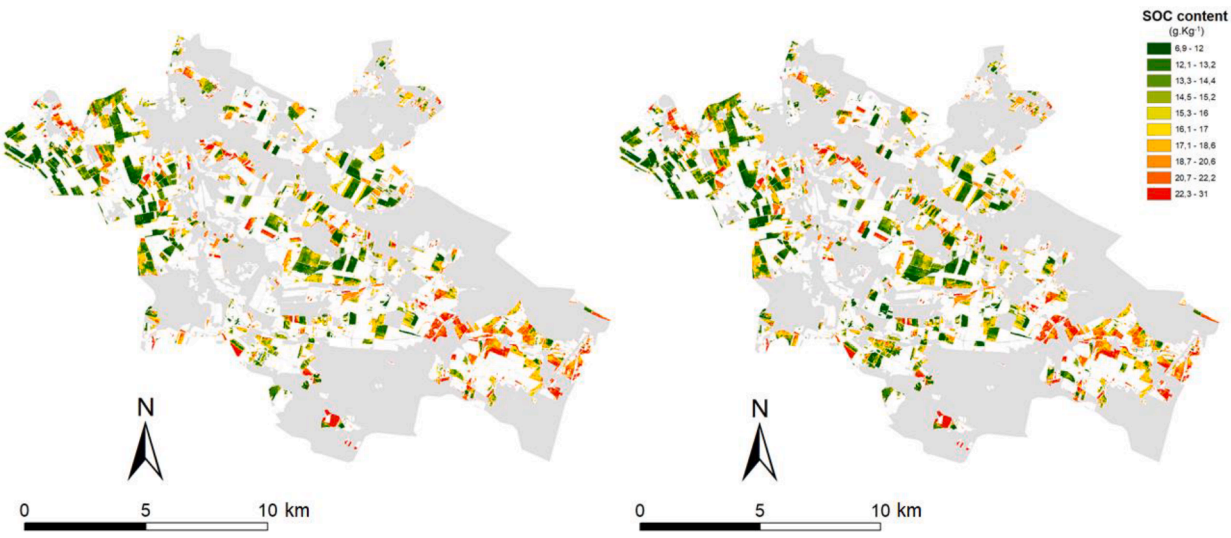

Fig. 10. Maps of SOC contents derived from the 4-date mosaics obtained from the Best areal/driest date compromise (right) and from the BGP (left) (grey areas are non-agricultural areas, white areas are unpredicted vegetated fields).

properties (e.g., Stevens et al., 2010; Gomez et al., 2012; Vaudour et al., 2016), such index might not be the most adequate for creating a temporal mosaic of bare soil for the purpose of soil surface properties prediction.

As the use of NDVI may generate confusion with tree shadow, cloud shadow and low hanging clouds, Diek et al. (2017) proposed to use the BSI index rather than NDVI. Nevertheless, while slightly better than the NDVI-based, none of the mosaics obtained from a per-pixel approach driven by the BSI vegetation index allowed an acceptable SOC prediction performance, whatever the number of included dates and the BSI threshold (Table 11).

In contrast, the mosaic obtained from a per-pixel approach driven by both the NDVI and NBR2 indices allowed acceptable SOC prediction performances, when using 4 dates, a NDVI-threshold of 0.35 and a NBR2-threshold of 0.053 (RPDcv = 1.42 and bare soil coverage of 9.31 km^2 ; Table 11), corroborating the results obtained by Castaldi et al. (2019b) using NBR2 values lower than 0.05. The NBR2 index, also defined by Van Deventer et al. (1997) as the "Normalized Difference Tillage index" (NDTI) for the Landsat TM, is likely to exclude the spectra of soil covered by straw or crop residues (Demattè et al., 2018) and, because of the proximity between mid-infrared bands and soil moisture absorptions, may also exclude spectra affected by high soil moisture (Castaldi et al., 2019b).

None of the mosaics obtained from a per-pixel approach driven by

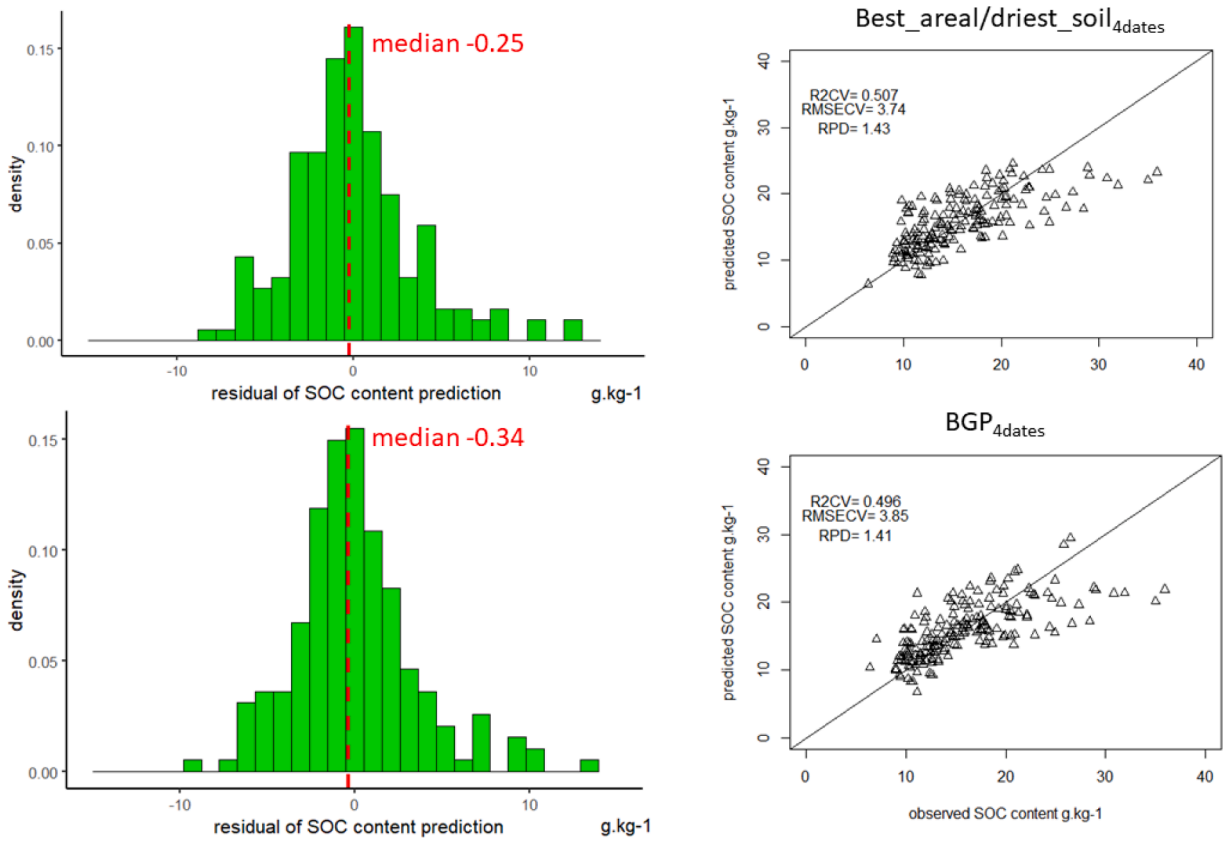

Fig. 11. Histograms of residuals and plots of predicted against observed SOC contents derived from the *Best areal_driest_date compromise* (up) and from the BGP_{4dates} (down).

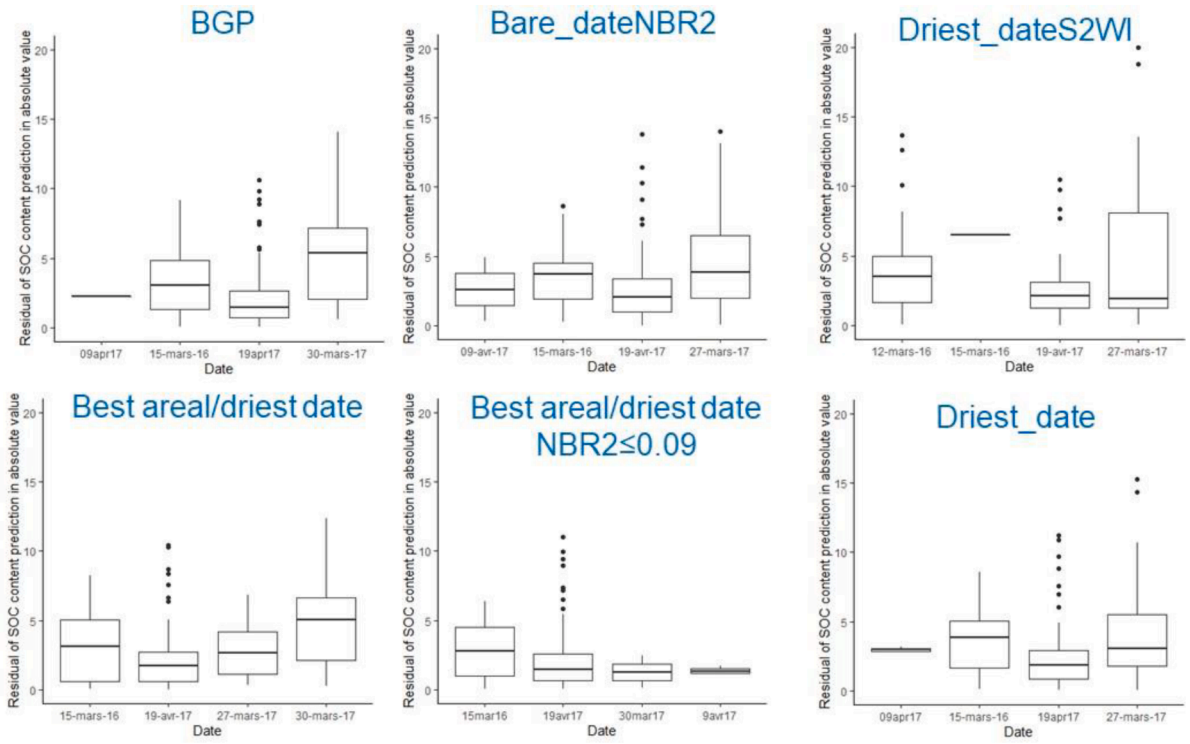

Fig. 12. Boxplots of residuals of predicted SOC contents (in absolute value) according to composing dates and methods.

both the NDVI and the S2WI moisture index yielded acceptable performances, whatever the number of included dates and the threshold of S2WI (Table 11). This lack of performance might be explained by the fact that, while this index proved capable of discriminating between very dry and very moist soils (Vaudour et al., 2019b), it might not well characterize intermediate situations.

The mosaic obtained from a per-pixel approach driven by both the NDVI index and the S1-derived soil moisture content θ yielded acceptable performances, for θ lower than 25% vol. and these lowest soil moisture values were derived from seven dates (RPDcv = 1,51 and 15.97 km^2; Table 11). Nevertheless, this mosaic allowed using only 42 soil samples for calibrating the SOC prediction model, so the results have to be considered with caution.

Finally, the mosaic obtained from a per-pixel approach driven by the NDVI, and thresholded NBR2 and S2WI indices allowed the best SOC prediction performances (RPDcv = 1.53; Table 11) but SOC was mapped over 16.6 km^2 only (Table 11). This performance suggests that models are sensitive to green vegetation, dry vegetation and moisture. Consequently, the construction of a temporal mosaic requires accounting for these 3 drivers.

4.2. Per-date approaches for mosaicking

As initiated by Diek et al (2016), it is important to consider the number of bare soil pixels to be included into the temporal mosaic. Similar to the per-pixel approaches, and whatever the approach used for creating a per-date mosaic, the predicted SOC maps obtained from these mosaics remained less accurate than the one produced using the single-date S2 data acquired on 19 April 2017 (RPDcv = 1.54, Table 4, Vaudour et al., 2019b). But in spite of this lower accuracy, the predicted SOC maps extended over more than twice the amount of bare soil pixels of the single-date S2 data acquired on 19 April 2017 (16.24 km^2, Table 4, Vaudour et al., 2019b). Consistently with a higher number of bare soil pixels included through a global indicator ranking, per-date approaches selected a much larger sample size for calibration (>154) than per-pixel (>40), and had a better representativeness of the study area.

When incorporating up to 4 dates, per-date approaches relying on ranking RPD resulted in acceptable performances, and close to acceptable with 5 dates (RPDcv = 1.38 and 39.73 km^2 of bare soil; Table 12). For BGP, validation figures provided in Table 13 shall be considered with caution as the same dataset (or a portion of it) was used to derive single and multidate performances.

Per-date approaches relying on ranking mean NDVI were unreliable, and this can be explained by no relationship between RPD and mean NDVI (Vaudour et al., 2019b). More refined approaches driven by both NDVI and NBR2 indices resulted in acceptable performances but for no >3 dates (RPDcv = 1.46 and 34.28 km^2 of bare soil; Table 12).

Per-date approaches relying on ranking the mean S2WI soil moisture index were unreliable, and this can be explained by the lack of sensitivity of S2WI. In contrast, per-date approaches relying on ranking the average S1-derived soil moisture resulted in acceptable performances, either for 3 dates only (RPDcv = 1.50 and 25.86 km^2 of bare soil; Table 12) or when considering the predicted area while ranking and discarding images having an average soil moisture higher than 25% vol.. The best results were obtained from 4 dates, all selected in Spring, including 1 date from the previous Spring, contributing to significant area increase (RPDcv = 1.43, RPD_{val} = 1.40 and 39.67 km^2 of bare soil, Tables 12&13).

4.3. Further researches

Whatever approach, incorporating the whole series into the model allowed to increase the calibration database and the mapped surface but did not always enable to obtain acceptable prediction performance. Because some dates are prone to spectral disturbances, namely presence of clouds and cloud shadows, presence of crop residues on surface, emerging green vegetation, soil moisture, soil surface roughness (Vaudour et al., 2019b), mosaicking should not be carried out with any whole series. Incorporating dates affected by some disturbances, such as soil surface roughness due to tillage operations, actually results into degraded mosaic performances. A further improvement of mosaicking approaches would therefore consist of considering both soil moisture and soil surface roughness information. Accounting for dry vegetation also matters, but the threshold above which NBR2 values need to be discarded is low and does not fulfill the need for extended mapping. Overall, it is advisable to perform a selection of the best suited dates, prior to temporal mosaicking. This study suggests to target the dates within reduced seasonal series marked by driest soils over several years.

5. Conclusion

Single date acquisitions hardly enable to derive SOC prediction over a sufficient percentage of the agricultural area. Bare soil areas can be maximized by aggregating multiple acquisition dates and this study confims that Sentinel-2 is particularly well suited to produce a composite multi-date bare soil image for predicting SOC content over cropland topsoils. For a cropland area monitored over two years and characterized by 3 or 4 years rotations, a limited number of dates could be incorporated within temporal mosaics yielding acceptable performances. At each date, only the bare soils were retained, but as crop vegetation coverage changes between dates, we finally obtained a substantial proportion of bare soil in the mosaics. The further incorporation of other Spring dates of further years covering the whole rotation would enable to answer the need for more extended bare soil area while maintaining an acceptable performance.

Because some dates are prone to spectral disturbances, mosaicking should not be carried out with any whole series, and only those dates in favour of best soil surface conditions shall be included. Two main sets of approaches seeking such conditions were conducted for Sentinel–2 images temporal mosaicking: the one, based on a per-pixel selection, was driven by soil surface characteristics, being bare soil, or bare dry soil, both deprived of green and/or dry vegetation; the other, based on a per-date selection, was driven either by the models performance with single-date, or by averaging soil surface indicators of bare soil, dry soil or a combination both.

Whatever approach used for creating a per-pixel mosaic, the predicted SOC maps obtained from such mosaics remained less accurate than the one produced using the best single-date S2 image, and some of them were even less extended following one or several thresholding steps, which limited the number of composing pixels fulfilling the pertaining conditions.

On the contrary, per-dates approaches were more likely to increase the mapped extent. Of the per-date approaches, the best trade-off between predicted area and model performance was achieved from the temporal mosaic driven by the S1-derived moisture content which enabled to more than double the predicted area.

This study suggests that a number of bare soil mosaics based on several indicators (moisture, bare soil, roughness…), preferably in combination, might maintain acceptable accuracies for SOC prediction whilst extending over larger areas than single-date images.

CRediT authorship contribution statement

Emmanuelle Vaudour: Conceptualization, Methodology, Formal analysis, Writing - review & editing, Funding acquisition, Supervision. **Cécile Gomez:** Conceptualization, Methodology, Writing - review & editing. **Philippe Lagacherie:** Conceptualization, Methodology, Writing - review & editing, Funding acquisition. **Thomas Loiseau:** Resources. **Nicolas Baghdadi:** Resources, Writing - review & editing. **Diego Urbina-Salazar:** Visualization. **Benjamin Loubet:** Resources, Writing - review & editing. **Dominique Arrouays:** Conceptualization, Methodology, Writing - review & editing, Funding acquisition.

Declaration of Competing Interest

The authors declare that they have no known competing financial interests or personal relationships that could have appeared to influence the work reported in this paper.

Acknowledgment

This work was supported by CNES, France and was carried out in the framework of the TOSCA "Cartographie Numérique des Sols (CNS)" program (grant number 3261-3264 CES Theia CartoSols) of the CNES. It also benefited support from the POLYPHEME project (grant number 200769/id5917) through the TOSCA program of the CNES and from the TELEMOS project through the *Programme National de Télédétection Spatiale* (PNTS, http://programmes.insu.cnrs.fr/pnts/), grant n° PNTS-2020-17). D. Arrouays is coordinator and P. Lagacherie is collaborator of the consortium GLASOILMAP supported by LE STUDIUM Loire Valley Institute for Advanced Studies through its LE STUDIUM Research Consortium Programme. Some data were retrieved from the FR-GRI long-term ICOS site.

Appendix A. Supplementary data

Supplementary data to this article can be found online at https://doi.org/10.1016/j.jag.2020.102277.

References

Arrouays, D., Horn, R., 2019. Soil Carbon - 4 per Mille - an introduction. Soil and Tillage Research 188, 1–2. https://doi.org/10.1016/j.still.2019.02.008.

Baetens, L., Desjardins, C., Hagolle, O., 2019. Validation of Copernicus Sentinel-2 Cloud Masks Obtained from MAJA, Sen2Cor, and FMask Processors Using Reference Cloud Masks Generated with a Supervised Active Learning Procedure. Remote Sensing 11, 433. https://doi.org/10.3390/rs11040433.

Baghdadi, N., El Hajj, M., Choker, M., Zribi, M., Bazzi, H., Vaudour, E., Gilliot, J.-M., Ebengo, D., 2018. Potential of Sentinel-1 Images for Estimating the Soil Roughness over Bare Agricultural Soils. Water 10, 131. https://doi.org/10.3390/w10020131.

Baghdadi, N., El Hajj, M., Zribi, M., Bousbih, S., 2017. Calibration of the water cloud model at C-band for winter crop fields and grasslands. Remote Sens. 9 (9), 969.

Baghdadi, N., Holah, N., Zribi, M., 2006. Calibration of the Integral Equation Model for SAR data in C-band and HH and VV polarizations. International Journal of Remote Sensing 27, 805–816. https://doi.org/10.1080/01431160500212278.

Baize, D., Jabiol, B., 2011. Guide pour la description des sols. Quae editions, Paris, France.

Bazzi H., Baghdadi N., El Hajj M., Zribi M., Belhouchette H., 2019. A Comparison of Two Soil Moisture Products S2MP and Copernicus-SSM over Southern France. Journal of Selected Topics in Applied Earth Observations and Remote Sensing, 10 pages, doi: 10.1109/JSTARS.2019.2927430.

Bellon-Maurel, V., Fernandez-Ahumada, E., Palagos, B., Roger, J.-M., McBratney, A., 2010. Critical review of chemometric indicators commonly used for assessing the quality of the prediction of soil attributes by NIR spectroscopy. TrAC Trends in Analytical Chemistry 29, 1073–1081. https://doi.org/10.1016/j.trac.2010.05.006.

Castaldi, F., Chabrillat, S., Don, A., van Wesemael, B., 2019a. Soil Organic Carbon Mapping Using LUCAS Topsoil Database and Sentinel-2 Data: An Approach to Reduce Soil Moisture and Crop Residue Effects. Remote Sensing 11, 2121. https://doi.org/10.3390/rs11182121.

Castaldi, F., Hueni, A., Chabrillat, S., Ward, K., Buttafuoco, G., Bomans, B., Vreys, K., Brell, M., van Wesemael, B., 2019b. Evaluating the capability of the Sentinel 2 data for soil organic carbon prediction in croplands. ISPRS Journal of Photogrammetry and Remote Sensing 147, 267–282. https://doi.org/10.1016/j.isprsjprs.2018.11.026.

Chenu, C., Angers, D.A., Barré, P., Derrien, D., Arrouays, D., Balesdent, J., 2018. Increasing organic stocks in agricultural soils: Knowledge gaps and potential innovations. Soil and Tillage Research. https://doi.org/10.1016/j.still.2018.04.011.

Crahet, M., 1992. Soil Map of the Versailles Plain. Scale 1:50 000. Institut National Agronomique Paris-Grignon, Grignon, Internal report.

Demattê, J.A.M., Fongaro, C.T., Rizzo, R., Safanelli, J.L., 2018. Geospatial Soil Sensing System (GEOS3): A powerful data mining procedure to retrieve soil spectral reflectance from satellite images. Remote Sensing of Environment 212, 161–175. https://doi.org/10.1016/j.rse.2018.04.047.

Demattê, J.A.M., Safanelli, J.L., Poppiel, R.R., Rizzo, R., Silvero, N.E.Q., Mendes, W. de S., Bonfatti, B.R., Dotto, A.C., Salazar, D.F.U., Mello, F.A. de O., Paiva, A.F. da S., Souza, A.B., Santos, N.V. dos, Maria Nascimento, C., Mello, D.C. de, Bellinaso, H., Gonzaga Neto, L., Amorim, M.T.A., Resende, M.E.B. de, Vieira, J. da S., Queiroz, L.G. de, Gallo, B.C., Sayão, V.M., Lisboa, C.J. da S., 2020. Bare Earth's Surface Spectra as a Proxy for Soil Resource Monitoring. Scientific Reports 10. Doi: 10.1038/s41598-020-61408-1.

Diek, S., Schaepman, M., de Jong, R., 2016. Creating Multi-Temporal Composites of Airborne Imaging Spectroscopy Data in Support of Digital Soil Mapping. Remote Sensing 8, 906. https://doi.org/10.3390/rs8110906.

Diek, S., Fornallaz, F., Schaepman, M., de Jong, M., 2017. Barest Pixel Composite for Agricultural Areas Using Landsat Time Series. Remote Sensing 9, 1245. https://doi.org/10.3390/rs9121245.

El Hajj, M., Baghdadi, N., Zribi, M., Bazzi, H., 2017. Synergic use of Sentinel-1 and Sentinel-2 images for operational soil moisture mapping at high spatial resolution over agricultural areas. Remote Sensing 9, 1292. https://doi.org/10.3390/rs9121292.

Gallo, B., Demattê, J., Rizzo, R., Safanelli, J., Mendes, W., Lepsch, I., Sato, M., Romero, D., Lacerda, M., 2018. Multi-Temporal Satellite Images on Topsoil Attribute Quantification and the Relationship with Soil Classes and Geology. Remote Sensing 10, 1571. https://doi.org/10.3390/rs10101571.

Geladi, P., Kowalski, B.R., 1986. Partial least squares regression: a tutorial. Analytica Chimica Acta 185, 1–17.

Loiseau, T., Chen, S., Mulder, V.L., Román Dobarco, M., Richer-de-Forges, A.C., Lehmann, S., Bourennane, H., Saby, N.P.A., Martin, M.P., Vaudour, E., Gomez, C., Lagacherie, P., Arrouays, D., 2019. Satellite data integration for soil clay content modelling at a national scale. International Journal of Applied Earth Observation and Geoinformation 82, 101905. https://doi.org/10.1016/j.jag.2019.101905.

Loubet, B., Laville, P., Lehuger, S., Larmanou, E., Fléchard, C., Mascher, N., Genermont, S., Roche, R., Ferrara, R.M., Stella, P., Personne, E., Durand, B., Decuq, C., Flura, D., Masson, S., Fanucci, O., Rampon, J.-N., Siemens, J., Kindler, R., Gabrielle, B., Schrumpf, M., Cellier, P., 2011. Carbon, nitrogen and Greenhouse gases budgets over a four years crop rotation in northern France. Plant and Soil 343, 109–137. https://doi.org/10.1007/s11104-011-0751-9.

Gholizadeh, A., Žižala, D., Saberioon, M., Borůvka, L., 2018. Soil organic carbon and texture retrieving and mapping using proximal, airborne and Sentinel-2 spectral imaging. Remote Sensing of Environment 218, 89–103. https://doi.org/10.1016/j.rse.2018.09.015.

Gomez, C., Lagacherie, P., Coulouma, G., 2012. Regional predictions of eight common soil properties and their spatial structures from hyperspectral Vis–NIR data. Geoderma 189–190, 176–185. https://doi.org/10.1016/j.geoderma.2012.05.023.

Inglada, J., Vincent, A., Arias, M., Tardy, B., Morin, D., Rodes, I., 2017. Operational High Resolution Land Cover Map Production at the Country Scale Using Satellite Image Time Series. Remote Sensing 9, 95. https://doi.org/10.3390/rs9010095.

Joanes, D.N., Gill, C.A., 1998. Comparing measures of sample skewness and kurtosis. Journal of the Royal Statistical Society: Series D (The Statistician) 47, 183–189. https://doi.org/10.1111/1467-9884.00122.

Minasny, B., Malone, B.P., McBratney, A.B., Angers, D.A., Arrouays, D., Chambers, A., Chaplot, V., Chen, Z.-S., Cheng, K., Das, B.S., Field, D.J., Gimona, A., Hedley, C.B., Hong, S.Y., Mandal, B., Marchant, B.P., Martin, M., McConkey, B.G., Mulder, V.L., O'Rourke, S., Richer-de-Forges, A.C., Odeh, I., Padarian, J., Paustian, K., Pan, G., Poggio, L., Savin, I., Stolbovoy, V., Stockmann, U., Sulaeman, Y., Tsui, C.-C., Vågen, T.-G., van Wesemael, B., Winowiecki, L., 2017. Soil carbon 4 per mille. Geoderma 292, 59–86. https://doi.org/10.1016/j.geoderma.2017.01.002.

Minasny, B., McBratney, A.B., Bellon-Maurel, V., Roger, J.-M., Gobrecht, A., Ferrand, L., Joalland, S., 2011. Removing the effect of soil moisture from NIR diffuse reflectance spectra for the prediction of soil organic carbon. Geoderma 167-168, 118–124. https://doi.org/10.1016/j.geoderma.2011.09.008.

Noirot-Cosson, P.E., Vaudour, E., Gilliot, J.M., Gabrielle, B., Houot, S., 2016. Modelling the long-term effect of urban waste compost applications on carbon and nitrogen dynamics in temperate cropland. Soil Biology and Biochemistry 94, 138–153. https://doi.org/10.1016/j.soilbio.2015.11.014.

R Development Core Team, 2015. The Comprehensive R Archive Network. The R Foundation for Statistical Computing, Wirtschaft Universitat, Vienna, Austria. http://www.r-project.org/. (Accessed 10 December 2020).

Rienzi, E.A., Mijatovic, B., Mueller, T.G., Matocha, C.J., Sikora, F.J., Castrignanò, A., 2014. Prediction of Soil Organic Carbon under Varying Moisture Levels Using Reflectance Spectroscopy. Soil Science Society of America Journal 78 (958). https://doi.org/10.2136/sssaj2013.09.0408.

Rogge, D., Bauer, A., Zeidler, J., Mueller, A., Esch, T., Heiden, U., 2018. Building an exposed soil composite processor (SCMaP) for mapping spatial and temporal characteristics of soils with Landsat imagery (1984–2014). Remote Sensing of Environment 205, 1–17. https://doi.org/10.1016/j.rse.2017.11.004.

Selige, T., Böhner, J., Schmidhalter, U., 2006. High resolution topsoil mapping using hyperspectral image and field data in multivariate regression modeling procedures. Geoderma 136, 235–244. https://doi.org/10.1016/j.geoderma.2006.03.050.

Stevens, A., Udelhoven, T., Denis, A., Tychon, B., Lioy, R., Hoffmann, L., van Wesemael, B., 2010. Measuring soil organic carbon in croplands at regional scale using airborne imaging spectroscopy. Geoderma 158, 32–45. https://doi.org/10.1016/j.geoderma.2009.11.032.

Tziolas, N., Tsakiridis, N., Ben-Dor, E., Theocharis, J., Zalidis, G., 2020. Employing a Multi-Input Deep Convolutional Neural Network to Derive Soil Clay Content from a Synergy of Multi-Temporal Optical and Radar Imagery Data. Remote Sensing 12, 1389. https://doi.org/10.3390/rs12091389.

Van Deventer, A.P., Ward, A.D., Gowda, P.H., Lyon, G.J., 1997. Using Thematic Mapper data to identify contrasting soil plains and tillage practices. Photogrammetric Engineering & Remote Sensing 63 (1), 87–93.

Vaudour, E., Gilliot, J.M., Bel, L., Lefevre, J., Chehdi, K., 2016. Regional prediction of soil organic carbon content over temperate croplands using visible near-infrared airborne hyperspectral imagery and synchronous field spectra. International Journal of Applied Earth Observation and Geoinformation 49, 24–38. https://doi.org/10.1016/j.jag.2016.01.005.

Vaudour, E., Baghdadi, N., Gilliot, J.M., 2014a. Mapping tillage operations over a peri-urban region using combined SPOT4 and ASAR/ENVISAT images. International Journal of Applied Earth Observation and Geoinformation 28, 43–59. https://doi.org/10.1016/j.jag.2013.11.005.

Vaudour, E., Gilliot, J.M., Bel, L., Bréchet, L., Hamiache, J., Hadjar, D., Lemonnier, Y., 2014b. Uncertainty of soil reflectance retrieval from SPOT and RapidEye multispectral satellite images using a per-pixel bootstrapped empirical line atmospheric correction over an agricultural region. International Journal of Applied Earth Observation and Geoinformation 26, 217–234. https://doi.org/10.1016/j.jag.2013.07.003.

Vaudour, E., Gomez, C., Fouad, Y., Lagacherie, P., 2019a. Sentinel-2 image capacities to predict common topsoil properties of temperate and Mediterranean agroecosystems. Remote Sensing of Environment 223, 21–33. https://doi.org/10.1016/j.rse.2019.01.006.

Vaudour, E., Gomez, C., Loiseau, T., Baghdadi, N., Loubet, B., Arrouays, D., Ali, L., Lagacherie, P., 2019. The Impact of Acquisition Date on the Prediction Performance of Topsoil Organic Carbon from Sentinel-2 for Croplands 17.

Viscarra Rossel, R.A., Walvoort, D.J.J., McBratney, A.B., Janik, L.J., Skjemstad, J.O., 2006. Visible, near infrared, mid infrared or combined diffuse reflectance spectroscopy for simultaneous assessment of various soil properties. Geoderma 131, 59–75. https://doi.org/10.1016/j.geoderma.2005.03.007.

Wehrens, R., Mevik, B.-H., 2007. The pls package: principal component and partial least squares regression in R.

Wold, S., 1978. Cross-Validatory Estimation of the Number of Components in Factor and Principal Components Models. Technometrics 20, 397–405. https://doi.org/10.1080/00401706.1978.10489693.

Wold, S., Sjöström, M., Eriksson, L., 2001. PLS-regression: a basic tool of chemometrics. Chemometrics and Intelligent Laboratory Systems 58, 109–130. https://doi.org/10.1016/S0169-7439(01)00155-1.

Wuertz, D., Setz, T., Chalabi, Y., Maechler, M., 2020. Package fBasics, Rmetrics - Markets and Basic Statistics. Version 3042.89.1, CRAN repository, 130 p.

World Reference Base (WRB), 2014. World reference base for soil resources. A framework for international classification, correlation and communication. Food and Agriculture Organization of the United Nations, Rome, Italy, pp. 1–128.

Zaouche, M., Bel, L., Vaudour, E., 2017. Geostatistical mapping of topsoil organic carbon and uncertainty assessment in Western Paris croplands (France). Geoderma Regional 10, 126–137. https://doi.org/10.1016/j.geodrs.2017.07.002.

Žížala, D., Minařík, R., Zádorová, T., 2019. Soil Organic Carbon Mapping Using Multispectral Remote Sensing Data: Prediction Ability of Data with Different Spatial and Spectral Resolutions. Remote Sensing 11 (2947). https://doi.org/10.3390/rs11242947.